NPS ME-92-005

NAVAL POSTGRADUATE SCHOOL

Monterey, California

Thermoelastic Stresses in Multi-Layered Media in Non-Uniform Temperature Fields

by

DAVID SALINAS

YOUNG W. KWON

and

MICHAEL J. NEIBERT

Prepared for:
Naval Weapons Support Center
Code 0211
Crane, Indiana 47522

Naval Postgraduate School
Monterey, California

Rear Admiral R. W. West, Jr.
Superintendent

H. Shull
Provost

This report was prepared for the Naval Weapons Support Center, Code 0211, Crane, Indiana, 47522, using funds provided by the Naval Postgraduate School, Monterey, California, 93943-5100.

This report was prepared by:

DAVID SALINAS
Assoc. Prof. of Mech. Engng.

YOUNG W. Kwon
Assist. Prof. of Mech. Engng.

MICHAEL J. NEIBERT
Lt., U.S. Navy

Reviewed by:

MATTHEW D. KELLEHER
Chairman, Dept. of Mech. Engng.

Released by:

PAUL J. MARTO
Dean of Research

SECURITY CLASSIFICATION OF THIS PAGE

REPORT DOCUMENTATION PAGE

1a. REPORT SECURITY CLASSIFICATION: UNCLASSIFIED	1b. RESTRICTIVE MARKINGS
2a. SECURITY CLASSIFICATION AUTHORITY	3. DISTRIBUTION / AVAILABILITY OF REPORT: APPROVED FOR PUBLIC RELEASE: UNLIMITED DISTRIBUTION
2b. DECLASSIFICATION / DOWNGRADING SCHEDULE	
4. PERFORMING ORGANIZATION REPORT NUMBER(S): NPS ME-92-005	5. MONITORING ORGANIZATION REPORT NUMBER(S)
6a. NAME OF PERFORMING ORGANIZATION: DEPT. OF MECH. ENGN'G. / 6b. OFFICE SYMBOL (If applicable): ME	7a. NAME OF MONITORING ORGANIZATION
6c. ADDRESS (City, State, and ZIP Code): NAVAL POSTGRADUATE SCHOOL MONTEREY, CA 93943-5100	7b. ADDRESS (City, State, and ZIP Code)
8a. NAME OF FUNDING / SPONSORING ORGANIZATION: NAVAL POSTGRADUATE SCH. / 8b. OFFICE SYMBOL (If applicable)	9. PROCUREMENT INSTRUMENT IDENTIFICATION NUMBER
8c. ADDRESS (City, State, and ZIP Code)	10. SOURCE OF FUNDING NUMBERS: PROGRAM ELEMENT NO. / PROJECT NO / TASK NO / WORK UNIT ACCESSION NO.

11. TITLE (Include Security Classification)
THERMOELASTIC STRESSES IN MULTI-LAYERED MEDIA IN NON-UNIFORM TEMPERATURE FIELDS

Thermoelastic Stresses in Multi-Layered Media in Non-Uniform Temperature Fields

12. PERSONAL AUTHOR(S)

13a. TYPE OF REPORT	13b. TIME COVERED	14. DATE OF REPORT (Year, Month, Day)	15. PAGE COUNT
FINAL REPORT	FROM JAN 92 TO DEC 92	1992 DEC 31	43

16. SUPPLEMENTARY NOTATION

17. COSATI CODES			18. SUBJECT TERMS (Continue on reverse if necessary and identify by block number)
FIELD	GROUP	SUB-GROUP	THERMOELASTIC STRESSES, MULTILAYERED MEDIA, NONUNIFORM TEMPERATURE FIELDS

19. ABSTRACT (Continue on reverse if necessary and identify by block number)

The objective of this investigation is to determine the shear and peeling stresses in a multilayered media in a nonuniform temperature field. The temperature field is obtained by a finite element solution of the energy equation with a flux generation term in one of the media layers. The resulting thermoelastic stresses are then obtained from a finite element model which uses a recently developed beam element with only displacement degrees of freedom. Compared to the standard beam element with rotational degrees of freedom, this element without rotational degrees of freedom more readily provides displacement continuity along interfaces between medial layers. As a result of the differences in properties such as Young's modulii, Poisson's ratio, and coefficients of thermal expansion, thermoelastic stresses develop when the multilayered media is subjected to a thermal environment. In particular, the model is used in this investigation to determine the sheae and

20. DISTRIBUTION / AVAILABILITY OF ABSTRACT: ☒ UNCLASSIFIED/UNLIMITED ☐ SAME AS RPT ☐ DTIC USERS	21. ABSTRACT SECURITY CLASSIFICATION	
22a. NAME OF RESPONSIBLE INDIVIDUAL: DAVID SALINAS	22b. TELEPHONE (Include Area Code): 408-656-3426	22c. OFFICE SYMBOL: ME/SA

DD FORM 1473, 84 MAR — 83 APR edition may be used until exhausted. All other editions are obsolete.

SECURITY CLASSIFICATION OF THIS PAGE

* U.S. Government Printing Office: 1986—606-24.

19. (continuation)

peeling stresses along media interfaces that occur in electronic chip packages which consist of a chip connected to a ceramic base by a thin layer of lead solder. The thickness and length dimensions of the various media layers are different. A study to determine the individual effects of both geometry and material property parameters was undertaken. Observations regarding system behavior are then presented. Numerical solutions fot some simple cases are compared to analytical solutions to verify the accuracy of the numerical model.

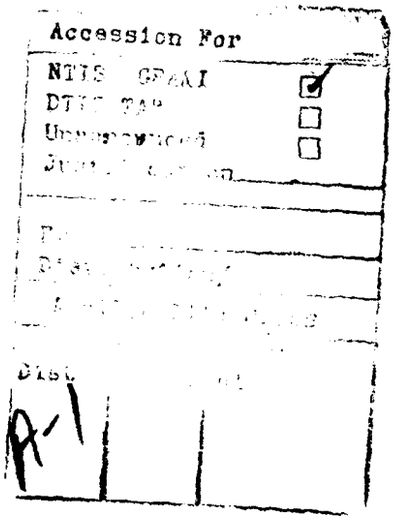

Thermoelastic Stresses in Multi-Layered Media in Non-Uniform Temperature Fields

D. Salinas, Y.W. Kwon and M. Neibert

CHAPTER 1. INTRODUCTION

Because of the mismatch in mechanical and thermal properties, thermoelastic stresses develop in multi-layered media subjected to temperature fields. In a 1925 paper, Timoshenko [1] presented the solution for bending of a bi-metallic strip (a thermostat) in an uniform temperature field. Closed form expressions for bending stresses, in terms of strip thicknesses, Young's modulii, and coefficients of thermal expansion, are given. Timoshenko noted that the 'distribution of shearing stress along the bearing surface cannot be determined in an elementary way' and observed that the magnitude of the shearing stresses may be of the same order as that of the bending stresses, and additionally, normal stresses along the interface exist near the ends of the strip.

In a 1944 paper, Goland and Reissner [2] determined the shear and peeling stresses along the interface of a cemented lap joint connecting two plates subjected to axial loads at their ends. Temperature effects were not included. The closed form analytical solutions show that the peeling stresses along the interface and the bending stresses near the cemented lap joint are as much as four times greater than the axial stresses away from the bonded interface. The shear stresses along the bonded interface are but slightly less than the axial stresses away from the bonded interface. Peak peeling and shear stresses occur at the joint edges. All stresses depend on the joint dimensions and the stiffness properties of the plates.

Subsequent investigators considered generalizations of the problem of multi-layered media in uniform temperature fields. In a comprehensive article on the subject, Suhir [3] summarizes the works of others as well as his own on the behavior of bi-material and tri-material assembled electronic packages in an uniform temperature field, or is subjected to applied axial load. The results show that for the bi-material assembly, the maximum peeling and shear stresses along the bonding interface occurs at the outer edges. The article covers fatigue, fracture, thermal shock, debonding, and thermoplastic failures. Equations for stresses are obtained from several models. It is shown that the stresses depend upon the axial and interfacial compliances of the assembly layers. The middle bonding layer in the tri-material assembly may extend over any fraction of the upper and lower layers. The article concludes with a list of about 240 references on the subject is provided. Suhir's own model is very general and includes most effects. However it is restricted to the case of multi-layered media in uniform temperature fields.

The present work generalizes the problem to that of a multi-layered structure in a transient and non uniform temperature field as might occur during the start of an electronic device. The formulation consists of two finite element codes, one for determination of the transient thermal field and the other for the determination of the transient bending, shear and peeling stresses resulting thereof. The finite element stress formulation utilizes a recently developed element which provides for axial and lateral displacement continuity. The results of the stress code are in good agreement with existing solutions [1,3] to problems with uniform temperature fields.

CHAPTER 2 FORMULATION OF THE MODEL

The problem at hand is to determine the stresses in a tri-material body subjected to a temperature field. In order to solve for the stresses in a tri-material system, the problem was partitioned into two parts, a thermal part to determine a temperature field, and a thermoelastic part to determine stresses due to a temperature field.

Formulation of the Thermal Problem

The temperatures in the thermal part of the problem depend upon material properties, system geometry, and the convective boundary conditions. In particular, the properties which enter into thermal behavior include the thermal coefficients of expansion, and the coefficients of thermal condition. The thermal behavior is governed by Laplace's equation

$$\nabla\cdot(k\nabla\phi) + q''' = 0 \qquad (x,y) \in A \tag{1}$$

where T(x,y) is the temperature field, q'''(x,y) is the volumetric heat source. Equation (1) is supplemented with convective boundary conditions along the top, bottom and right surfaces,

$$-k\frac{\partial T}{\partial n} = h(t - T_\infty) \tag{2}$$

and the symmetry condition

$$\frac{\partial T}{\partial n} = 0 \tag{3}$$

along the left (center line) boundary as shown in Figure 2.1.

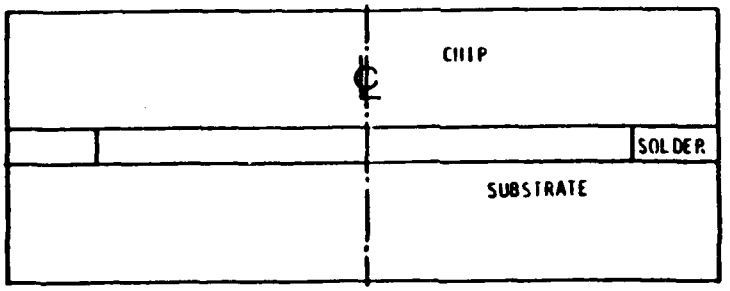

Figure 2.1 Geometry of a Trimaterial System

Equation (1) is transformed into a system of linear algebraic equations using the Galerkin form of the finite element method (FEM). In accordance with the finite element method, the rectangular domain of the structure is partitioned into the discrete mesh shown in figure 2.2.

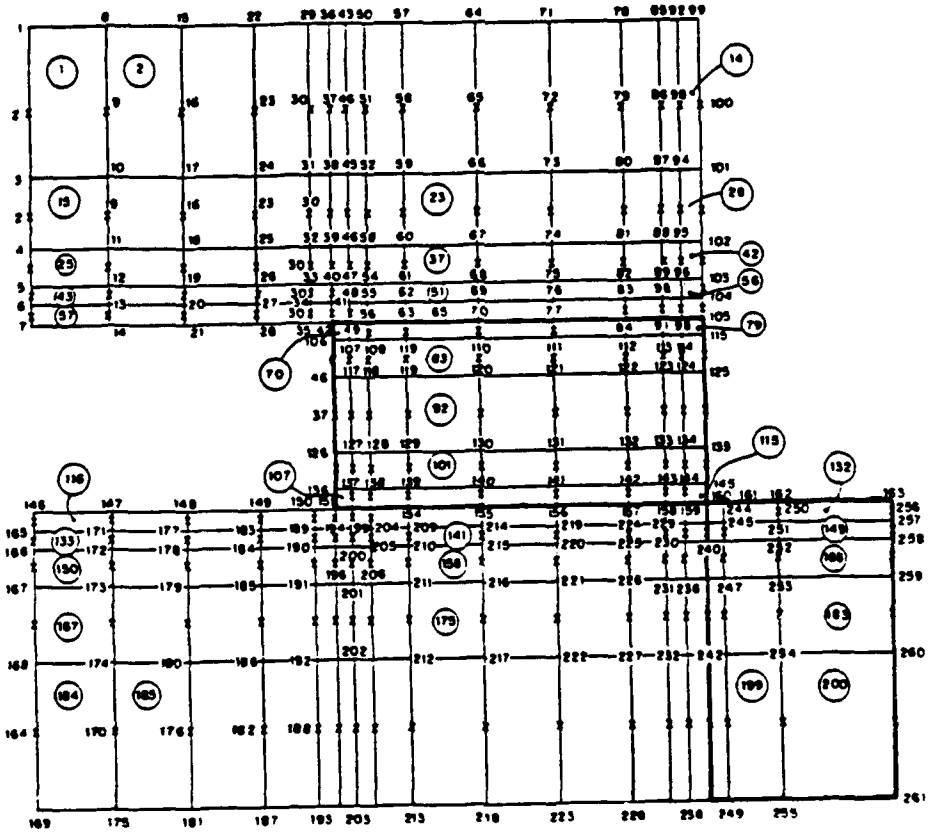

Figure 2.2 A Finite Element Mesh of the Trimaterial Medium

A piecewise linear approximation $\bar{T}(x,y)$ for temperature $T(x,y)$ is constructed as

$$T = \bar{T} = \{N\}^T\{T\} \tag{4}$$

where $T(x,y)$ is the exact solution of Eq.(1), $\bar{T}$ is the FEM approximate solution, $\{N\}^T$ is the row vector of linear shape functions, and $\{T\}$ is the column vector of nodal temperatures. A residual function, R, which is a measure of the error between T and it's approximation $\bar{T}$ is defined by

$$R(x,y) = \nabla\cdot(k\nabla\bar{T}) - q''' \tag{5}$$

Substituting Eq.(4) into Eq.(5) yields the residual

$$R(x,y) = \nabla\cdot[k\nabla(\{N\}^T\{T\})] - q'''(x,y) \tag{6}$$

Finally, the system of linear algebraic equations is obtained from the othogonalization of the residual function with each of the N_i ($i = 1,\ldots,n$) shape functions. That is,

$$\int_A \mathbf{N}R\,dA = \int_A \mathbf{N}\{\nabla\cdot[k\nabla(\mathbf{N}^T\mathbf{T}) - q'''\]\}dA = 0 \tag{7}$$

where a change from { } notation to bold character notation has taken place. Using Gauss's theorem, the above equation becomes

$$A = \int_A \nabla N [k \nabla (N^T)] \, dA \tag{10}$$

and the final 'excitation' vector term, say Q, is

$$Q = \int_A N q''' \, dA \tag{11}$$

Thus, after combining the first and third terms into F, where

$$F = (B + Q) \tag{12}$$

Eq.(1) has been transformed into the system of linear algebraic equations

$$A\bar{T} = F \tag{13}$$

The solution of these equations yields the temperatures at each node of the grid. These equations are for the steady state problem. For the transient problem, a transient term is added to the right hand side of Eq.(1), that is,

$$\nabla \cdot (k \nabla T) + q''' = \alpha \frac{\partial T}{\partial t} \tag{14}$$

where α is the specific heat of the material. Proceeding as before, Eq.(13) becomes

$$C\dot{T} = -AT + \dot{F} \tag{15}$$

where the C matrix resulting from the added $\alpha(\partial T/\partial t)$ term is given by

$$C = \int_A \alpha N N^T \, dA \tag{16}$$

In this case, the nodal temperatures are functions of time, that is $\bar{T}(t)$.

The stress formulation

A brief description of the FEM formulation for stresses follow. In Figure 2.3, each element has six degrees of freedom, axial displacements at the four corner points, and lateral displacements at the two ends. An advantage of the element is that axial and lateral displacement continuity results.

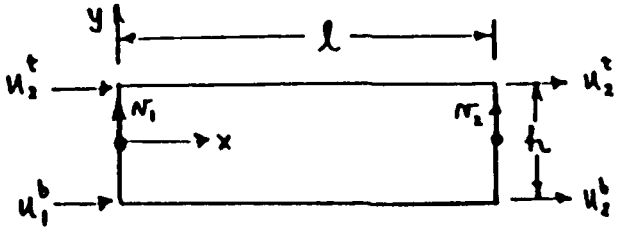

Figure 2.3 A typical element with 6 degrees of freedom

The axial displacement field u(x,y) is assumed to be linear in both the axial and transverse directions. That is,

$$u(x,y) = \sum_{i=1}^{2} N_i(x)\left[H_1(y)\, u_i^b + H_2(y)\, u_i^t\right] \tag{17}$$

Superscripts b and t on the nodal displacements refer to bottom and top displacements respectively. The linear shape functions N_i and H_i are given by

$$H_1(y) = \frac{h-y}{h} \qquad H_2 = \frac{y}{h} \qquad N_2(x) = \frac{l-x}{l} \qquad N_2 = \frac{x}{l} \tag{18}$$

where l and h are the length and height of a beam element. The lateral displacement field is given by

$$v(x) = \sum_{i=1}^{2} N_i(x)\, v_i \tag{19}$$

The strain-displacement relations are,

$$\epsilon_x = \frac{\partial u}{\partial x} = \frac{H_1(y)}{l}\left[u_2^b - u_1^b\right] + \frac{H_2(y)}{l}\left[u_2^t - u_1^t\right] \tag{20}$$

and

$$\gamma_{xy} = \frac{N_1(x)}{h}\left[u_1^t - u_1^b\right] + \frac{N_2(x)}{h}\left[u_2^t - u_2^b\right] + \frac{v_2 - v_1}{l} \tag{21}$$

Defining the axial displacement vector as

$$\{\delta_b\}^T = \langle\, u_1^b \quad u_1^t \quad u_2^b \quad u_2^t \,\rangle \tag{22}$$

and the stiffness matrix as

$$[K_B] = \int_0^l \int_o^h \{B\} E \{B\}^T dy\, dx \tag{23}$$

where the B vector is,

$$\{B\}^T = \langle\, \frac{\partial N_1}{\partial x} H_1 \quad \frac{\partial N_1}{\partial x} H_2 \quad \frac{\partial N_2}{\partial x} H_1 \quad \frac{\partial N_2}{\partial x} H_2 \rangle \tag{24}$$

and the force vector due to temperature as,

$$\{F_B\} = \frac{Eh}{6l} \int_0^l \int_0^h \{B\} E \alpha \Delta T\, dy\, dx \tag{25}$$

gives the bending matrix equations as,

$$[K_B]\ \{\delta_B\} = \{F_B\} \tag{26}$$

Equation (10) defines the bending behavior. Behavior due to shear is obtained as follows. Define the row vector of displacement degrees of freedom as

$$\{\delta_s\}^T = \langle u_1^b \quad u_1^t \quad v_1 \quad u_2^b \quad u_2^t \quad v_2 \rangle \tag{27}$$

The shear stiffness matrix is given by

$$[K_s] = \int_0^l \int_0^h \langle B' \rangle G \langle B' \rangle dy\,dx \tag{28}$$

where

$$\langle B' \rangle = \langle N_1 \frac{\partial H_1}{\partial y} \quad N_1 \frac{\partial H_2}{\partial y} \quad \frac{\partial N_1}{\partial x} \quad N_2 \frac{\partial H_1}{\partial y} \quad N_2 \frac{\partial H_2}{\partial y} \quad \frac{\partial N_2}{\partial x} \rangle \tag{29}$$

which gives the equations for shear behavior

$$[K_s]\{\delta_s\} = \{0\} \tag{30}$$

A reduced numerical integration scheme is used to compute the stiffness matrix due to shear. The matrix equations for bending and shear behavior are combined to give the stiffness equations for the system.

In order to understand the effects of material properties and geometric configuration on system behavior, a parametric study was undertaken. The study was conducted in two parts. In the first part, the effects of material properties, Youngs modulus (E), and thermal coefficient of expansion (α), were investigated. This is presented in Chapter 3. The second part considered the effects of system dimensions on system behavior. The effect of system geometry on system behavior consisted of two subparts. The first subpart considered the effect of midlayer thickness on system behavior. This is presented in Chapter 4. The second subpart considered the effect of midlayer length on system behavior. This is presented in Chapter 5. These studies were conducted for a uniform temperature field over the trimaterial system. Chapter 6 considers the effect of a nonuniform temperature field over a trimaterial system with application to electronic packages where the midlayer is the adhesive that joins the chip to a substrate.

CHAPTER 3 EFFECT OF MATERIAL PROPERTIES ON SYSTEM BEHAVIOR

In this study, the trimaterial system was subjected to a uniform temperature field 100 °C above the stress free temperature. Each of the three layers had a depth of 1 mm. The top and bottom layers had equal half-lengths of 10 mm., and the midlayer extened across half of this width as shown in Figure 2.1 below. The system is symmetric with respect to the y-axis.

The range of properties shown below in Table 3.1 were selected from the properties of materials which comprise trimaterial electronic packages, that is, ceramic substrates, silicon or arsenic chips, and solder adhesives. Although trimaterial configurations used in applications other than electronic packages may have significantly different properties than those considered here, it is expected that the observations made here remain valid. The quantitative would be different, but the behaviorial patterns would not change.

VALUE	E Youngs Modulus GPa	α Therm. Coeff. °C
Minimum	10	$1x10^{-6}$
Maximum	100	$400x10^{-6}$

Table 3.1 Range of property values

Effect of Youngs modulus

The first study investigated the effect of Youngs modulus on system behavior when both the temperature and coefficients of thermal expansion are uniform throughout the system and each of the layers have different Youngs modulii. As expected, the results show that no stresses develop.

Effect of thermal coefficient

In this study, the three layers had the same Youngs modulus, 100 GPa. Again, the temperature field was uniform for all layers at 100 °C above the stress free state. To determine the effects of thermal coefficient of expansion on system behavior, various combinations of thermal coefficients of expansion were selected for the three layers. The eleven cases shown in Table 3.2 below were considered.

Case	Material A	Material B	Material C
1	100	50	100
2	100	200	100
3	300	100	10
4	300	10	100
5	100	300	10
6	150	100	10
7	200	100	10
8	400	100	10
9	200	100	1
10	200	100	50
11	200	100	75

Table 3.2 Cases for study of effects of thermal coefficient of expansion

Cases 1 and 2. In cases 1 and 2, outer layers A and C have the same thermal expansion coefficients. For case 1, the midlayer has a lower coefficient of expansion than the outer layers, and in case 2 the midlayer has a higher thermal coefficient of expansion than the surrounding outer layers.

For case 1, the lower coefficient of expansion of the midlayer should cause the midlayer to expand along it's top and bottom interfaces. The shear and normal stress results presented in figure 3.1 shows that. These figures also show that these interface 'stretching' shear stresses are accompanied by interface peeling normal stresses. It is also seen that the shearing stresses, for the particular geometric configuration previously described, are three to six times larger than the normal stresses. It is also noted that the maximum shearing and normal stresses occur at the corner ends of the interfaces.

The results for case 2, wherein the midlayer had a higher thermal coefficient than the neighboring upper and lower layers, might have been anticipated from the results of case 1. Whereas the midlayer was previously being 'tensile' shear along its interfaces, it is now subjected to the opposite effect of 'compressive' shear stresses along its interfaces. The 'compressive' shear stresses are now accompanied by normal bearing stresses on the upper and botton surfaces of the midlayer. Again the magnitudes of the shearing stresses are three to six times larger than the normal stresses and the maximum magnitudes of stress occur at the corners of the

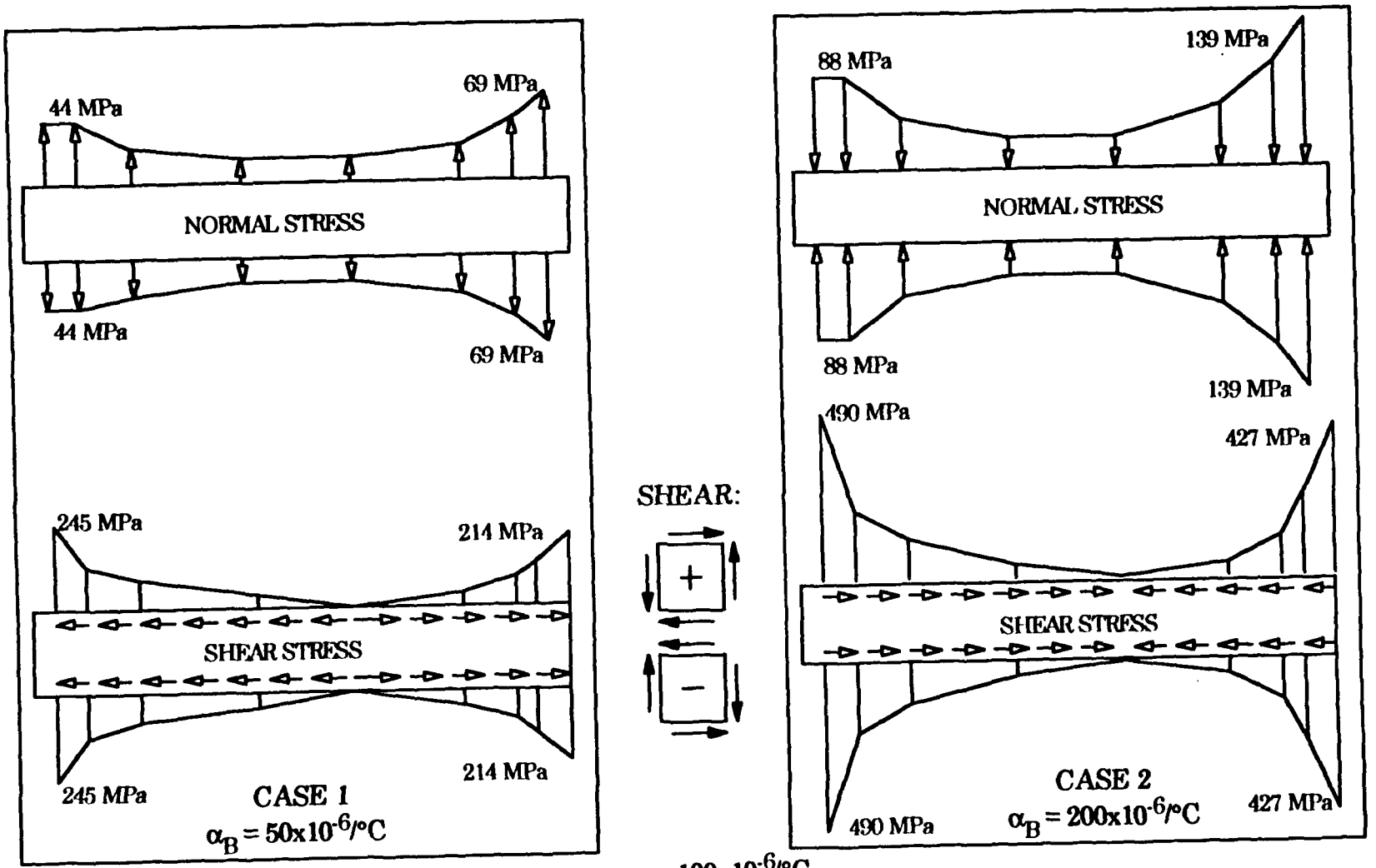

$\alpha_A = \alpha_C = 100x10^{-6}/°C$

$E_A = E_B = E_C$ 100 GPa

Figure 3.1 Shear And Normal Stresses On The Midlayer For Cases 1 And 2

midlayer. In both cases the maximum shear stresses occur at the innermost point of the midlayer and the maximum normal stress occurs at the outermost midlayer point.

Cases 3, 4 and 5. These cases were selected to assess the effect of the ordering of thermal coefficients as follows. In case 3, $\alpha_A > \alpha_B > \alpha_C$, that is, the coefficient of thermal expansion decrease from top to bottom of the trimaterial system. In case 4, the coefficients from top to mid to bottom layers were selected in the order, largest value: smallest value: mid value. In case 5, the order was changed to mid value: largest value: smallest value. The magnitudes of the thermal coefficients of expansion for all three cases are shown in figure 3.2.

The results from these three cases are presented in the same figure. A comparison of the results shows that

- The smallest shear and normal stresses occur for case 3, where the thermal coefficients of expansion decrease from the top to the bottom of the trimaterial system. In this case, the deformation o the medium is similar to that of pure bending. As a result, these stresses are significantly less than the stresses obtained in cases 4 and 5.

- In cases where the thermal coefficient of expansion of the midlayer is the largest or the smallest compared to those of the outer layers, the interface shear and normal stresses become large.

- When the thermal coefficient of expansion of the midlayer is the largest, the normal stress is a bearing stress and the shear stresses contract the midlayer as shown in case 5. On the other hand, the smallest thermal coefficient of expansion (case 4) causes the peeling normal stress at the interface and the shear stress in the opposite direction of that in case 5.

- Again in all cases, the interface shear stresses are significantly larger than the interface normal stresses.

Cases 3, 6, 7 , and 8. In this study, the thermal coefficients of expansion of the mid and bottom layers was held constant while the thermal coefficient of expansion of the top layer was varied as shown in figures 3.3 and 3.4. In all cases here, the coefficients of expansion had values decreasing fro top to bottom layer. With regard to the top layer whose thermal coefficient of expansion varied in decreasing order as follows: case 8 ($400\times10^{-6}/^{\circ}C$), case 3 ($300\times10^{-6}/^{\circ}C$), case 7 ($200\times10^{-6}/^{\circ}C$), and case 6 ($150\times10^{-6}/^{\circ}C$). The values of the thermal coefficient of expansion for the mid (B) and bottom layers (C), were fixed at $100\times10^{-6}/^{\circ}C$, and $10\times10^{-6}/^{\circ}C$ respectively.

The results of this study presented in figures 3.3 through 3.4 show the following.

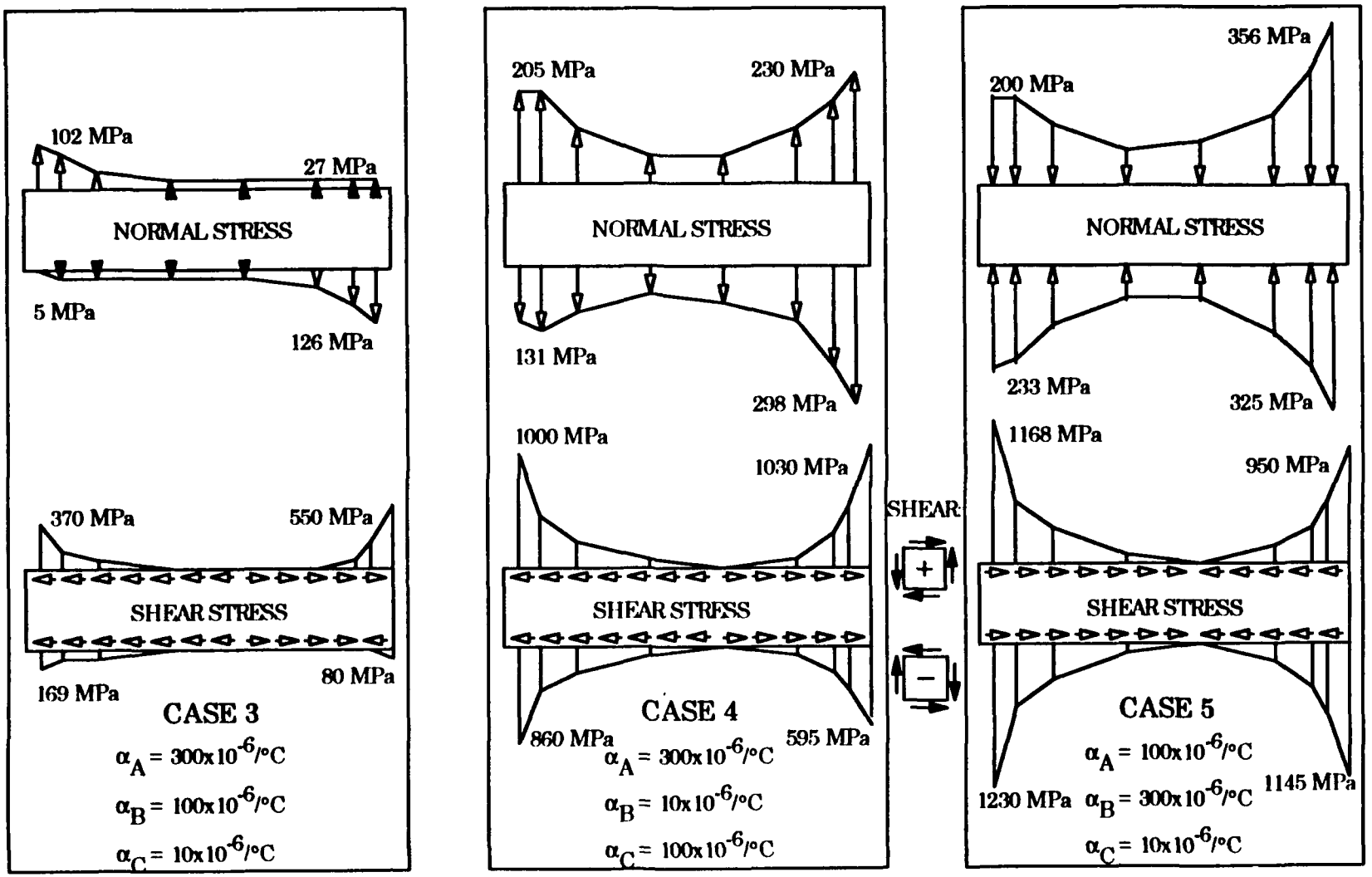

$E_A = E_B = E_C = 100$ GPa

Figure 3.2 Shear And Normal Stresses On The Midlayer For Cases 3, 4, And 5

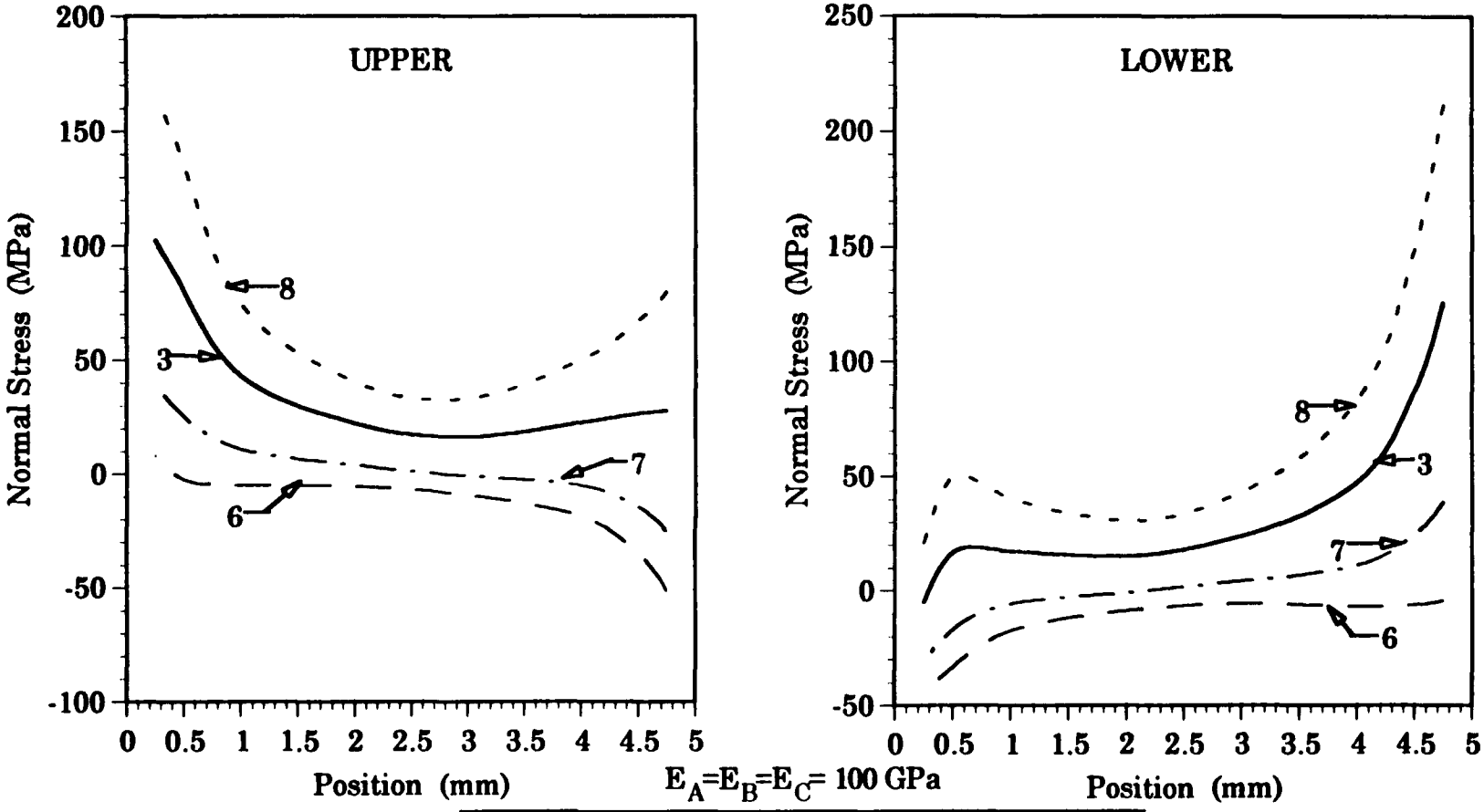

$E_A=E_B=E_C=$ 100 GPa

Case	α_A(x10^{-6}/°C)	α_B(x10^{-6}/°C)	α_C(x10^{-6}/°C)
3	300	100	10
6	150	100	10
7	200	100	10
8	400	100	10

Figure 3.3 Normal Stress At Interfaces For Cases 3, 6, 7, And 8

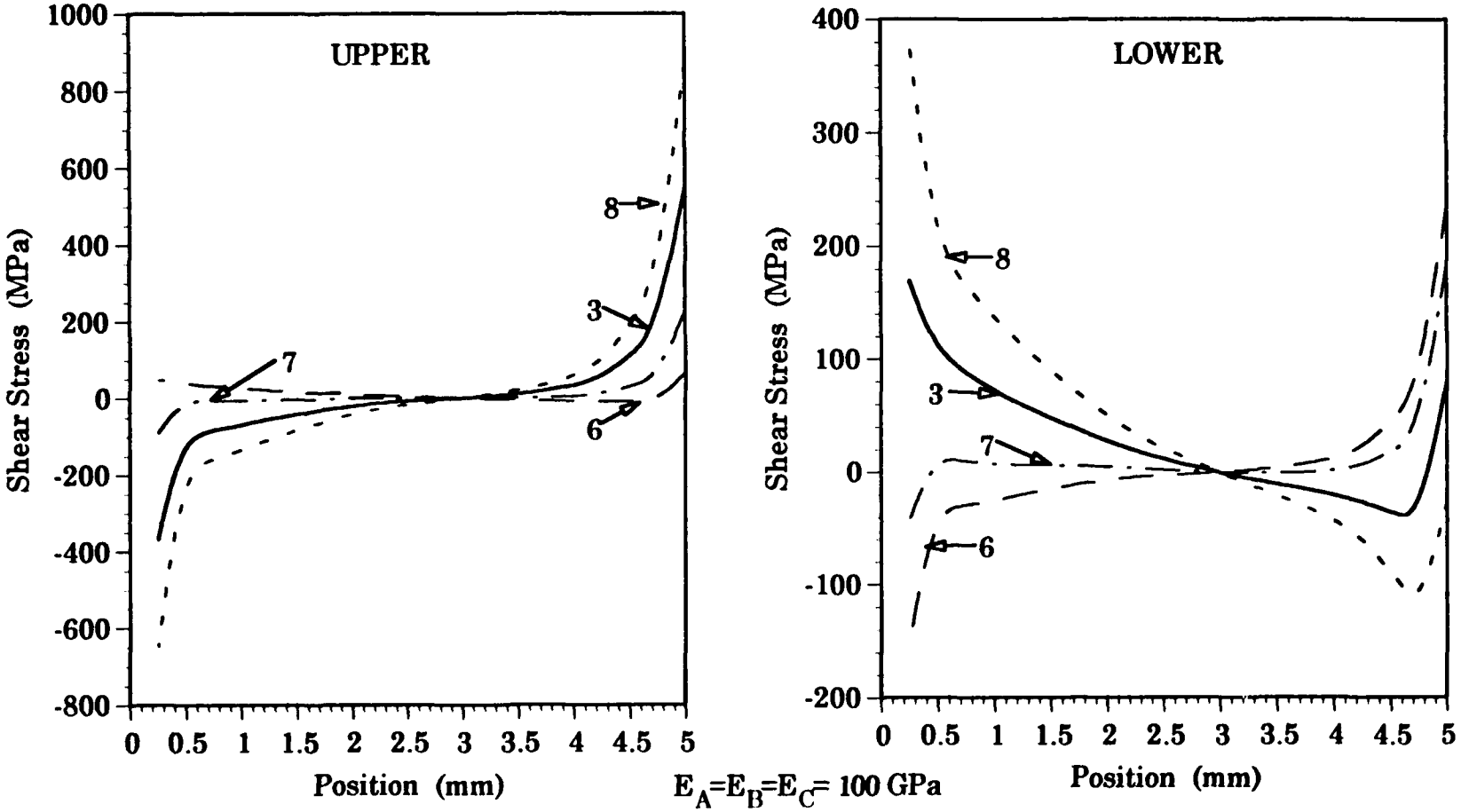

$E_A=E_B=E_C=100$ GPa

Case	$\alpha_A(\times10^{-6}/°C)$	$\alpha_B(\times10^{-6}/°C)$	$\alpha_C(\times10^{-6}/°C)$
3	300	100	10
6	150	100	10
7	200	100	10
8	400	100	10

Figure 3.4 Shear Stress At Interfaces For Cases 3, 6, 7, And 8

- The normal stresses are a maximum when the top layer has its largest thermal coefficient of expansion.

- These normal stresses decrease with decreasing value of thermal coefficient of expansion.

- If the thermal coefficient of expansion of the top layer is much larger than that of the midlayer, the interface normal stress is a peeling stress. On the other hand, if the thermal coefficients of expansion of top and middle layers are not so much different, the interface normal stress becomes a bearing stress.

- The maximum peeling stress occurs at the inner corner point of the upper interface surface and the outermost corner point of the lower interface surface.

- The normal stress distribution does not vary significantly away from its peak corner values.

- The interface shear stresses are significantly larger than the interface normal stresses.

- The shear stresses achieve their maximum values at the outer corner for the upper interface surface and the inner corner for the lower interface surface except for cases 6 and 7. The maximum shear stress on the upper interface surface is significantly larger than the maximum shear stress on the lower interface surface.

- The shear stresses achieve their maximum value when the thermal coefficient of expansion of the top layer is largest. The magnitudes of shear stresses decreases with decreasing magnitude of the coefficient of expansion of the top layer.

It should be noted that the results reported above are for the case where the lower layer has a fixed value of coefficient of thermal expansion below the values of thermal coefficient of expansion for the mid and upper layers. If the roles of upper and lower layers were reversed, that is, if the upper layer had a fixed thermal coefficient of expansion lower than the mid and bottom layers then the previous results would be valid simply by substituting the word 'upper' by 'lower' and the word 'lower' by 'upper'.

Cases 7, 9, 10, and 11. In this group of cases the effect of the decreasing values of thermal coefficient of expansion of an outer layer on system behavior was investigated. As shown in figures 3.5 and 3.6, the values of the thermal coefficient of expansion of the top and mid layers were fixed at $200\times10^{-6}/^{\circ}C$ and $100\times10^{-6}/^{\circ}C$ respectively, while the coefficient of thermal expansion of the bottom layer was varied from $75\times10^{-6}/^{\circ}C$ (case 11), $50\times10^{-6}/^{\circ}C$ (case 10), $10\times10^{-6}/^{\circ}C$ (case7) to $1\times10^{-6}/^{\circ}C$ (case 9). The results of this study, are presented in Figures 3.5 through 3.6 and are briefly summarized here.

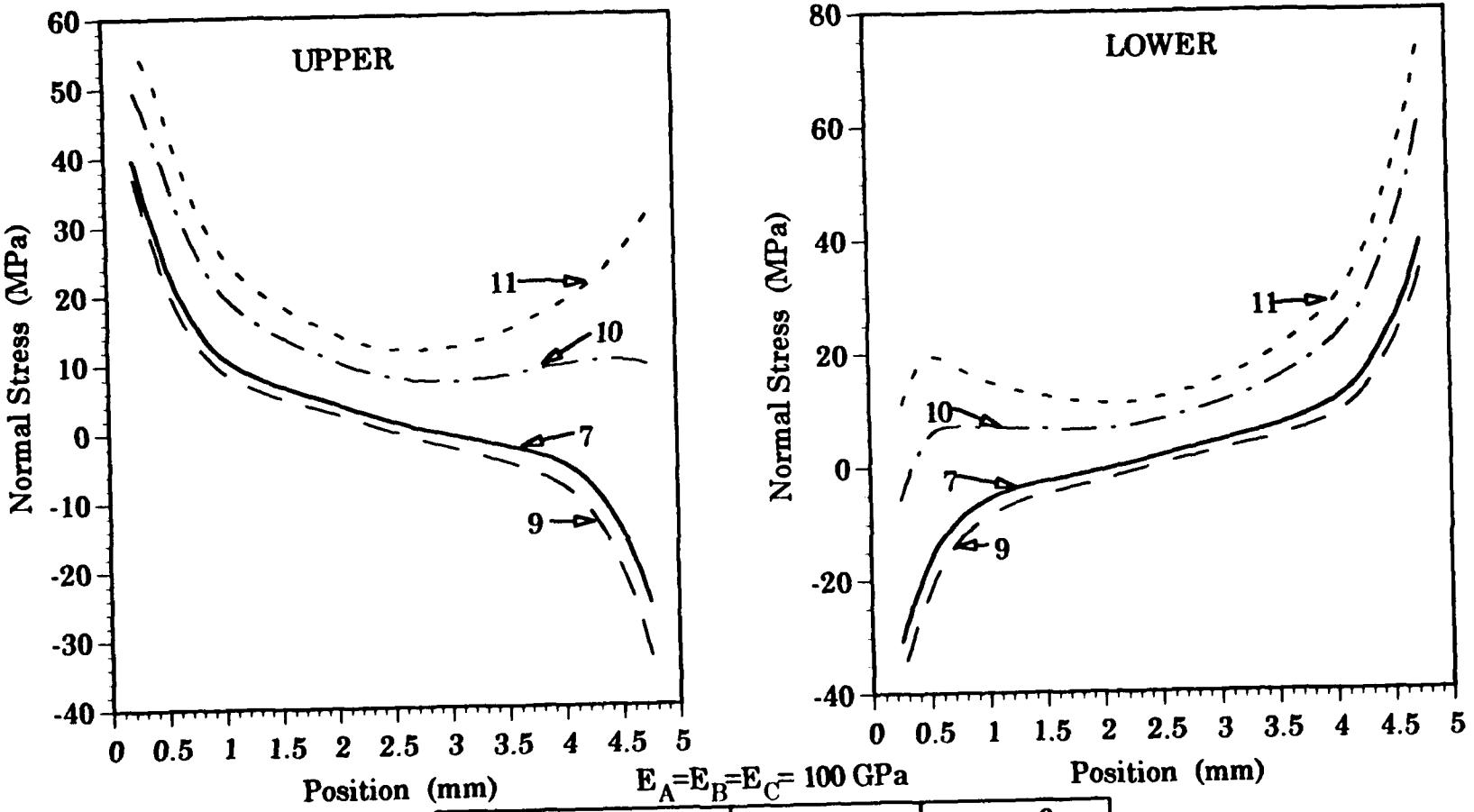

$E_A=E_B=E_C=100$ GPa

Case	$\alpha_A(\times10^{-6}/°C)$	$\alpha_B(\times10^{-6}/°C)$	$\alpha_C(\times10^{-6}/°C)$
7	200	100	10
9	200	100	1
10	200	100	50
11	200	100	75

Figure 3.5 Normal Stresses At Interfaces For Cases 7, 9, 10, And 11

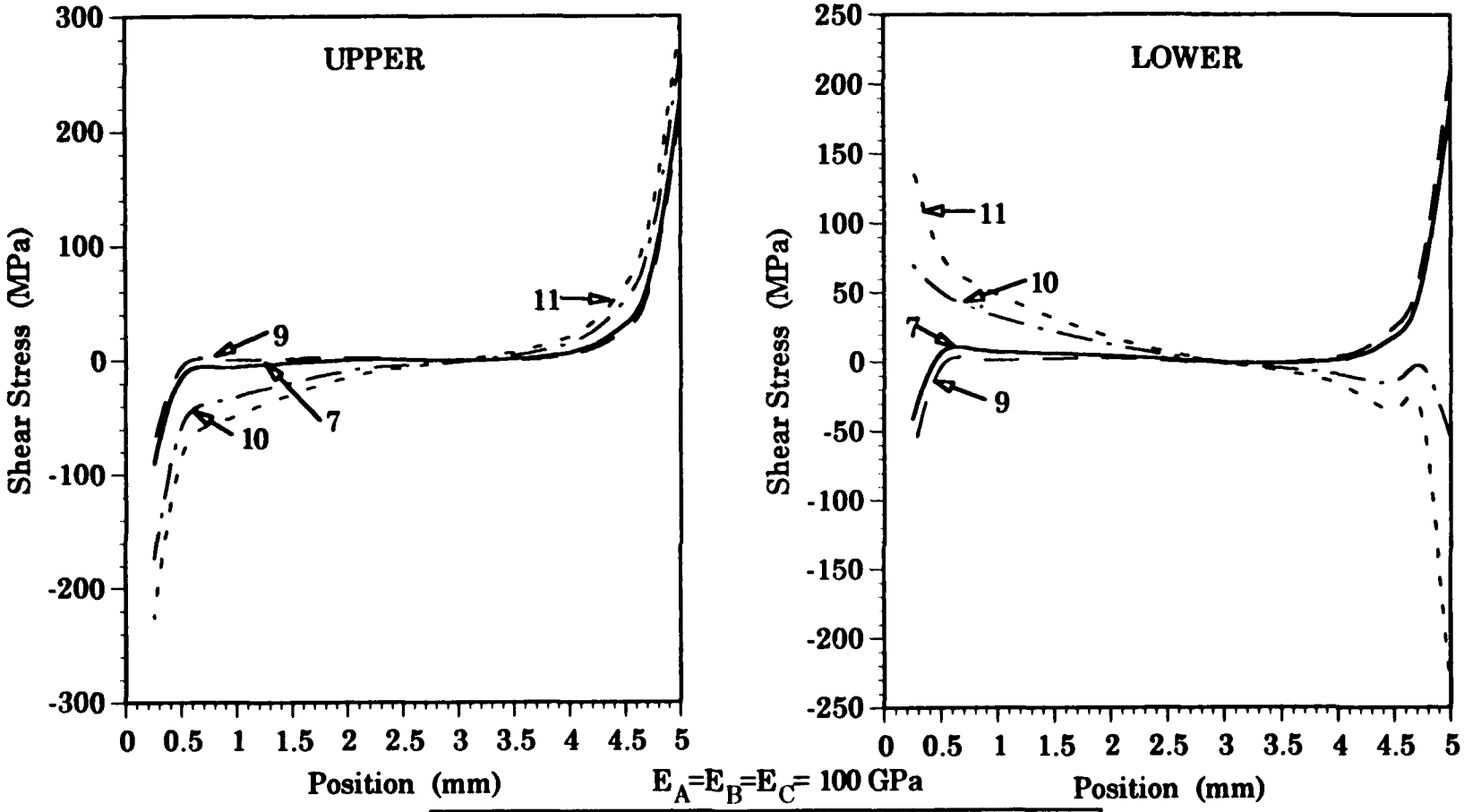

$E_A=E_B=E_C=100$ GPa

Case	$\alpha_A(\times10^{-6}/°C)$	$\alpha_B(\times10^{-6}/°C)$	$\alpha_C(\times10^{-6}/°C)$
7	200	100	10
9	200	100	1
10	200	100	50
11	200	100	75

Figure 3.6 Shear Stress At Interfaces For Cases 7, 9, 10, And 11

• Both the normal and shear stresses are significantly lower than in the previous study where the thermal coefficient of expansion for an outer layer took on increasing values.

• Again the interface shear stresses are significantly larger than the interface normal stresses. And again, the largest interface normal and shear stresses occur at the inner and outer corner points of the midlayer.

• As the value of the thermal coefficient of expansion decreased in the sequence case 11, case 10, case 7, case 9, the normal stresses at the left side of the upper interface surface were always peeling. The magnitude of these upper left inner corner peeling stresses decreased as the thermal coefficient of expansion of the bottom layer decreased.

• For cases 11 and 10, the normal stresses along the upper interface surface were always peeling stresses. However for cases 7 and 9, the normal stresses continue to decrease along the interface and became bearing stresses at the outer corner of the interface.

• Somewhat similar behavior with regard to normal stresses was observed for the lower interface surface. Here all the normal stresses were peeling at the outer corner, with decreasing magnitude as the thermal coefficient of expansion of the bottom layer decreased. At the inner corner of the lower interface surface, the normal stresses were bearing stresses with decreasing magnitude as the thermal coefficient of expansion of the bottom layer increased.

• In all cases the shear stresses along the upper interface surface changed direction along the interface from a maximum 'negative' value at the inner corner to a maximum 'positive' value at the outer corner. These shear stresses were of a local nature with very sharp decrease to insignificant stress magnitude over most of the interface length. The magnitude of the interface shear stresses decreased as the magnitude of the thermal coefficient of expansion decreased.

• On the lower interface surface, the shear stresses were of a very local type, with insignificant value everywhere except in the immediate area of the inner and outer corners. The shear stresses on the lower interface surface exhibit somewhat different behavior than the shear stresses on the upper interface surface. In the case of the upper interface, the shape of the shear stress distribution goes from a local maximum 'negative' value at the inner corner to a local maximum 'positive' value at the outer corner for all cases. In contrast, at the lower interface surface, the shear stress distribution for cases 11 and 10 goes from 'positive' to 'negative' values while cases 7 and 9 go from 'negative' to 'positive' values.

Apparently there is some value of the coefficient of thermal expansion of the bottom layer that results in this 'reversal' of shear stress behavior.

Summary of Effect of Thermal Coefficient of Expansion on System Behavior.

The study on the effect of thermal coefficient of expansion on system shows that overall

- The magnitudes of interface normal and shear stresses increase with the the increase of nonuniformity between the thermal coefficient of expansion of the individual layers.

- Interface shear stresses are significantly larger than interface normal stresses.

- Interface normal stresses may peeling or bearing depending on the values of the thermal coefficients of expansion.

- Both the normal and shear interace stresses are of an extremely local nature and are significant only in the immediate area of the corners of the interface.

It must be pointed out that the results obtained in the above study was for a given geometry of the trimaterial system. It is expected that these results would hold qualitatively for other system geometries. The next two study were conducted to show the effect of system geometry on system behavior.

CHAPTER 4. THE EFFECT OF MIDLAYER THICKNESS ON SYSTEM BEHAVIOR

In this chapter, the effects of midlayer thickness on system behavior is investigated. In this study all system properties (that is, Youngs modulii and thermal coefficients of expansion) and all system dimensions except midlayer thickness are held fixed. A series of computer runs were conducted for different values of the midlayer thickness. The following values are fixed. The modulus of each layer is 100 GPa. The coefficients of thermal expansion of the top, mid and bottom layers were taken as $100 \times 10^{-6}/^{\circ}C$, $300 \times 10^{-6}/^{\circ}C$, and $10 \times 10^{-6}/^{\circ}C$ respectively. The midlayer thickness for the 5 cases (5, 12, 13, 14, and 15) conducted are shown in Figure 4.1. In the 5, 12, 13, 14, 15 sequence the thickness of the midlayer decreases from 1mm to .05mm. Figure 4.1 also shows the other dimensions of the trimaterial system. Figures 4.2 through 4.7 show the results which are summarized below.

- For the particular case of thermal coefficients of expansion used in this study Figure 4.2 shows that the bearing normal stresses on both the upper and lower interfaces decrease as the thickness of the midlayer decreases. Moreover as the thickness decreases, the distribution becomes more uniform over the interface as well. In the case of an extremely thin midlayer as might result from a thin adhesive glue or solder, the normal stresses would only exist at the edges (corners) of the interface. Figures 4.2 through 4.4 present a comparison of normal stresses in all of these cases by dividing the maximum normal stress of the particular case with the maximum normal stress of all the cases, that is, case 5.

- Figures 4.5 shows the effect of midlayer thickness on the interface shear stresses. We note that the magnitude of the interface shear stress decrease as the thickness of the midlayer decreases. And again, as the midlayer thickness decreases, the distribution of interface shear stress becomes progressively more and more local in nature.

- Figures 4.6 and 4.7 presenting comparisons of interface normal and shear stresses show that the latter are two to three times greater. These figures show that the location of the maximum interface shear stress on the lower interface moves from the inner edge to the outer edge of the interface. On the upper interface surface the maximum shear stress remained at the inner edge of the interface. The maximum normal stresses always occurred at the inner edge for both the upper and lower interface.

- Figures 4.2 through 4.7 show that all interface stresses diminish as the thickness of the midlayer decreases.

Although these results were obtained for a particular fixed set of thermal coefficient properties, and layer lengths, it is expected that these results are valid qualitatively for other values of thermal coefficients of expansion and layer lengths.

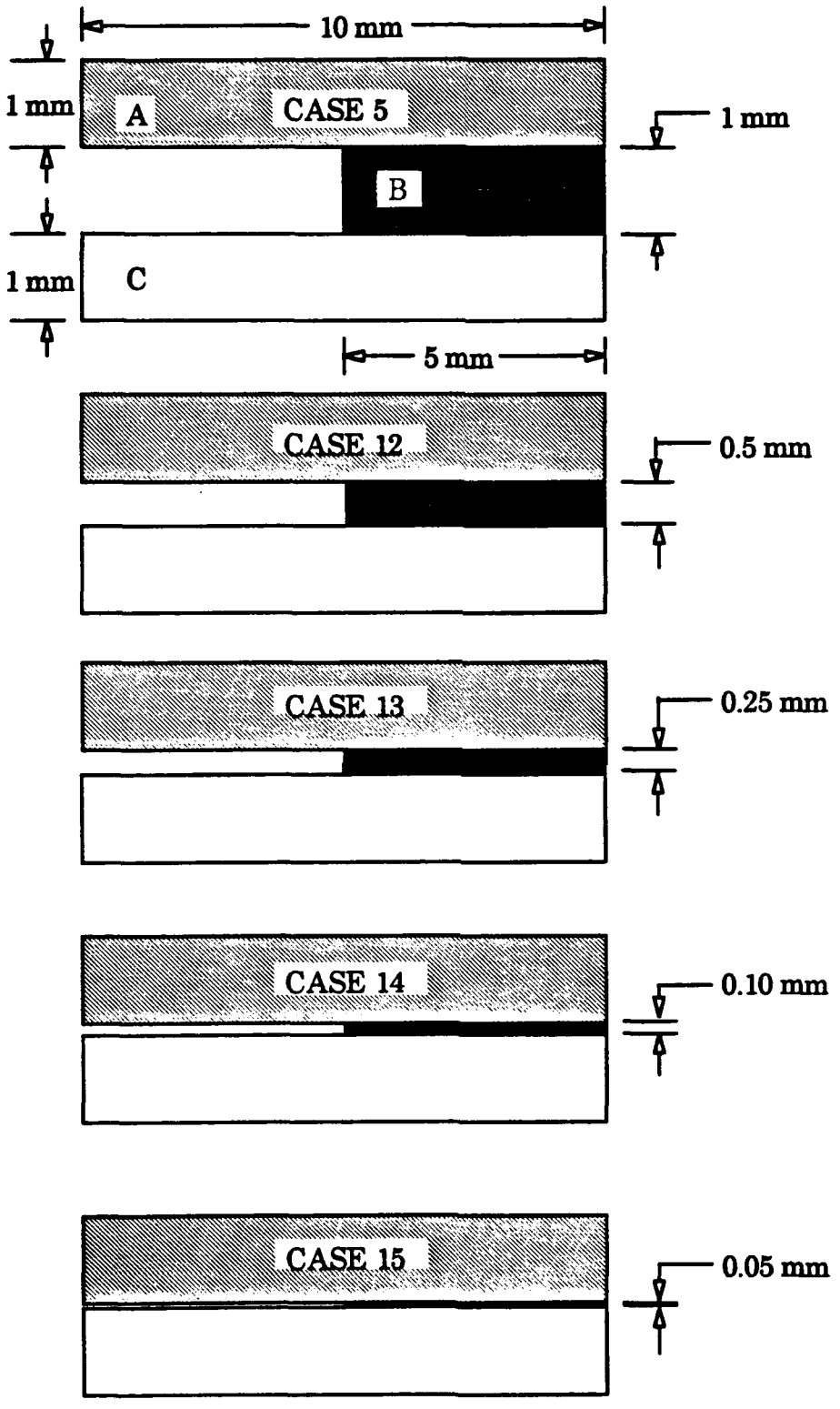

Figure 4.1 Tri-Material Configuration For Cases 5, 12, 13, 14, And 15

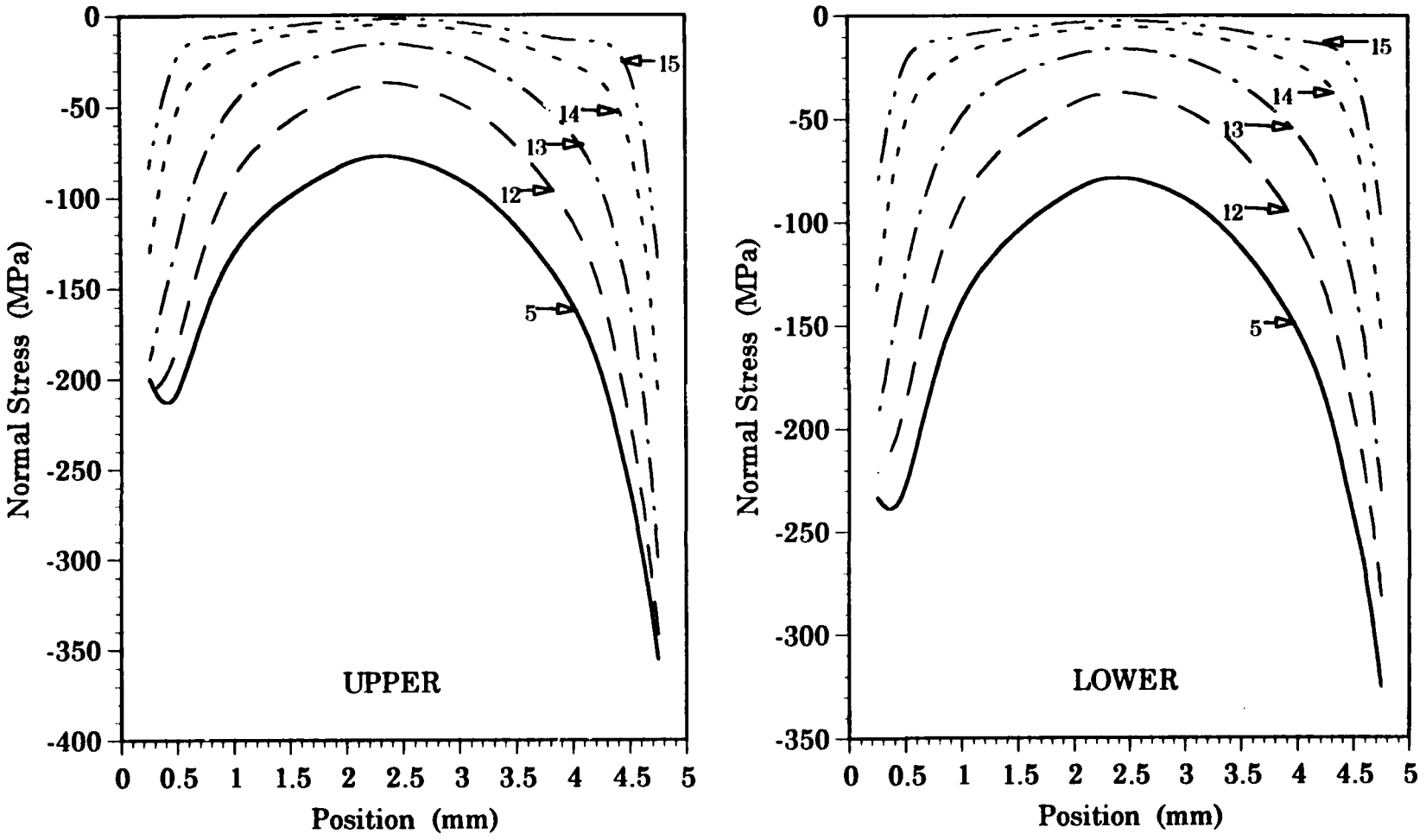

	Case 5	Case 12	Case 13	Case 14	Case 15
Material B Height (mm)	1	0.5	0.25	0.1	0.05

$\alpha_A = 100 \times 10^{-6}/°C$ $\alpha_B = 300 \times 10^{-6}/°C$ $\alpha_C = 10 \times 10^{-6}/°C$ $E_A = E_B = E_C = 100$ GPa

Figure 4.2 Normal Stresses At The Interfaces For Cases 5, 12, 13, 14, And 15

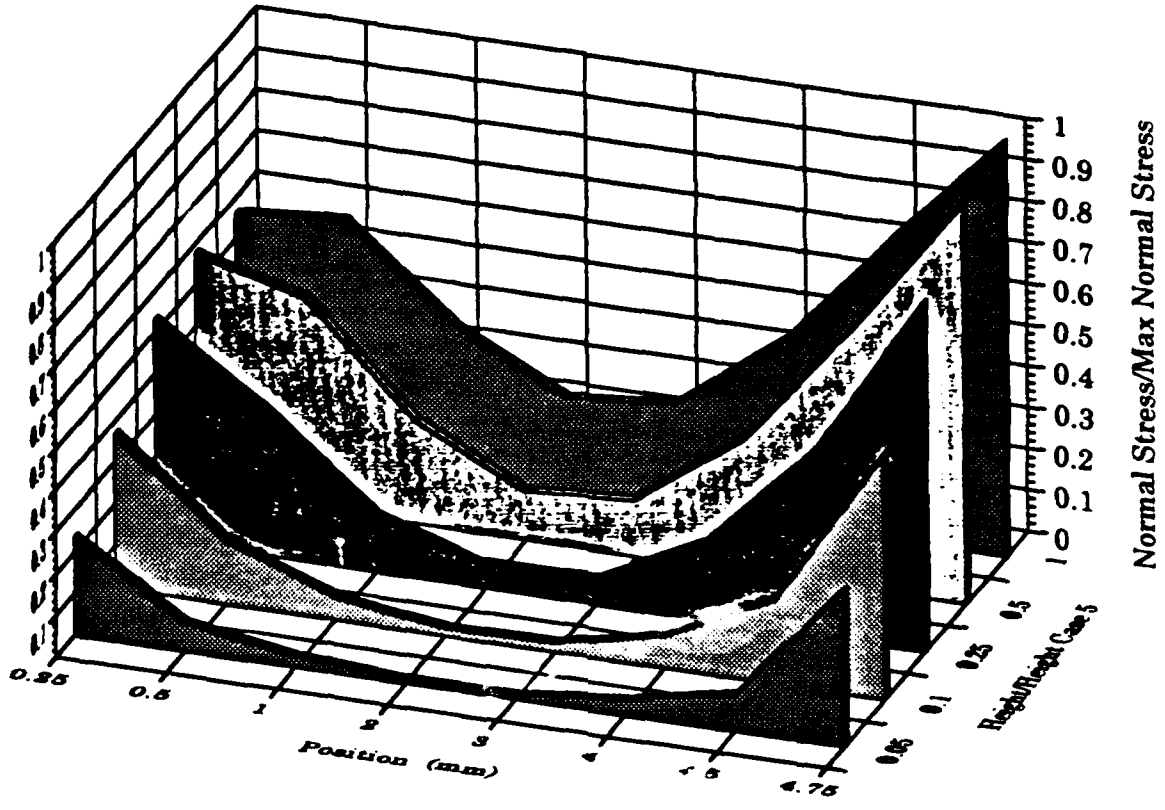

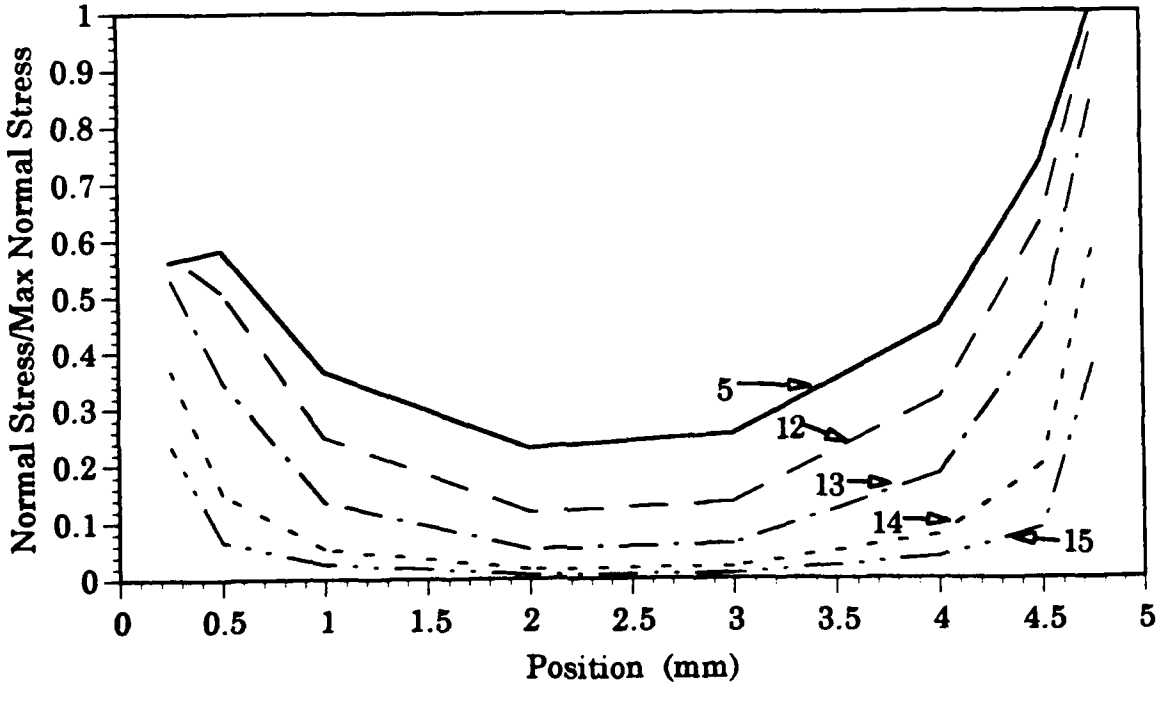

Figure 4.3 2-D And 3-D Plots Of Normal Stress/Maximum Normal Stress At The Upper Interface For Cases 5, 12, 13, 14, And 15

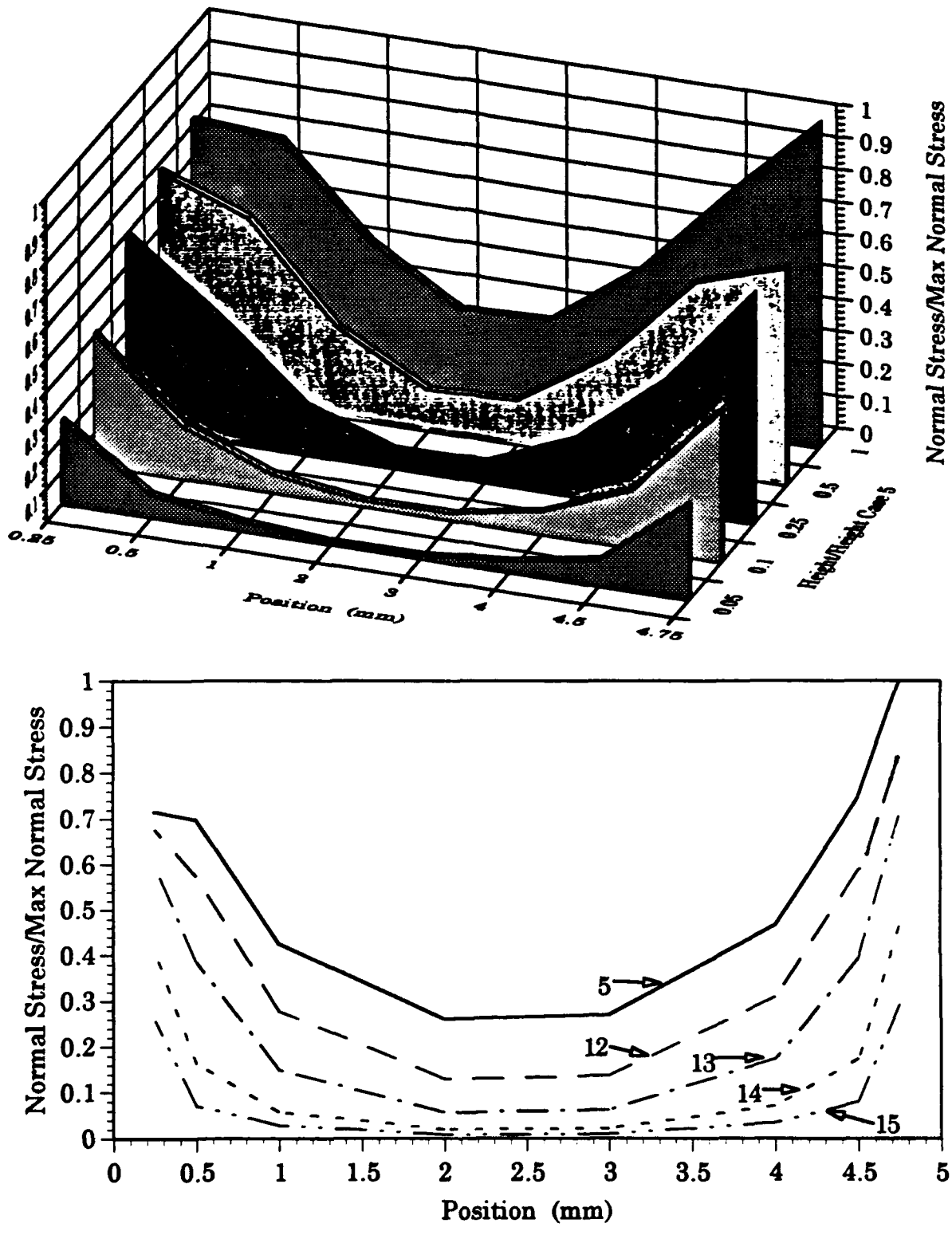

Figure 4.4 2-D And 3-D Plots Of Normal Stress/Maximum Normal Stress At The Lower Interface For Cases 5, 12, 13, 14, And 15

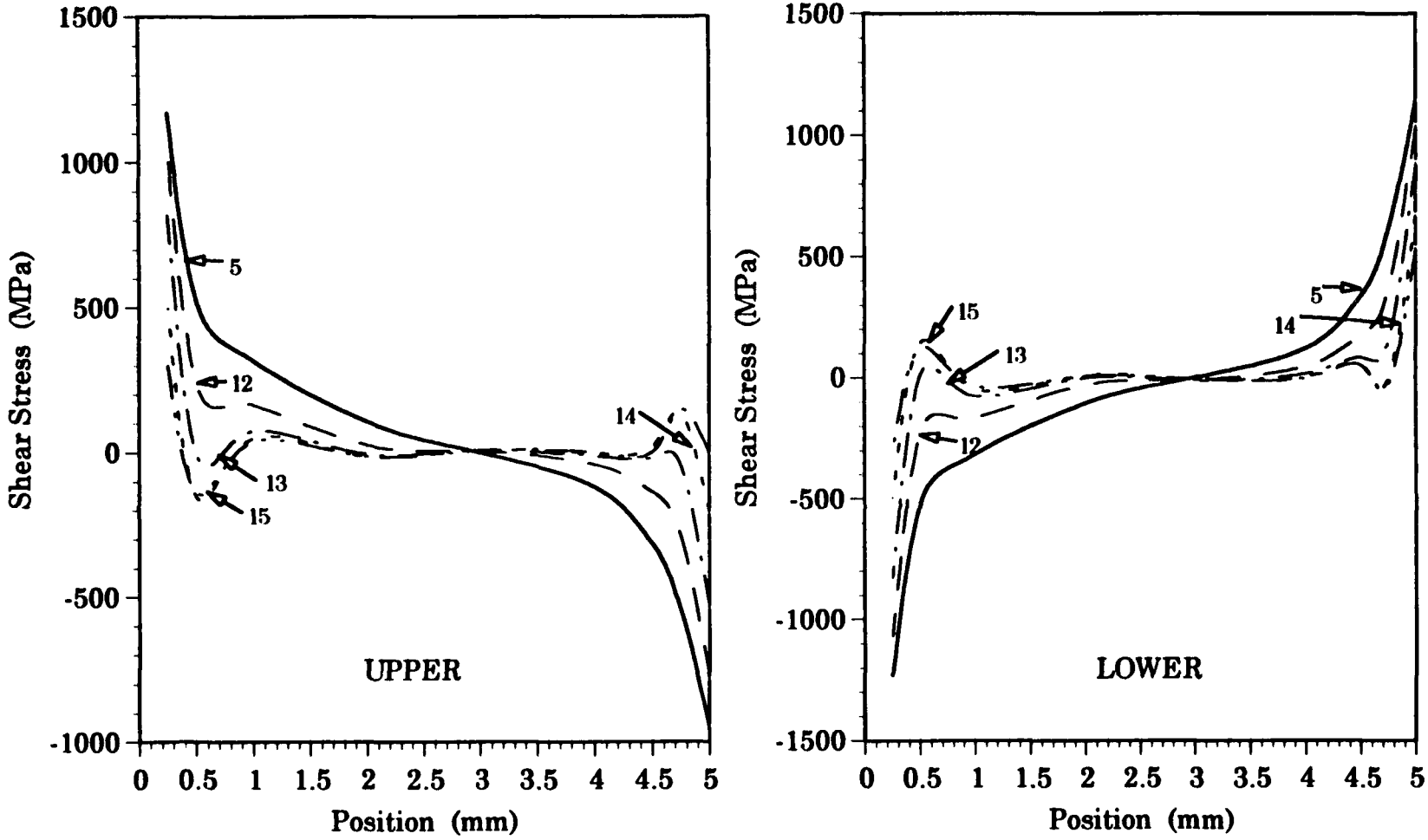

	Case 5	Case 12	Case 13	Case 14	Case 15
Material B Height (mm)	1	0.5	0.25	0.1	0.05

$\alpha_A = 100 \times 10^{-6}/°C$ $\alpha_B = 300 \times 10^{-6}/°C$ $\alpha_C = 10 \times 10^{-6}/°C$ $E_A = E_B = E_C = 100$ GPa

Figure 4.5 Shear Stresses At The Interfaces For Cases 5, 12, 13, 14, and 15

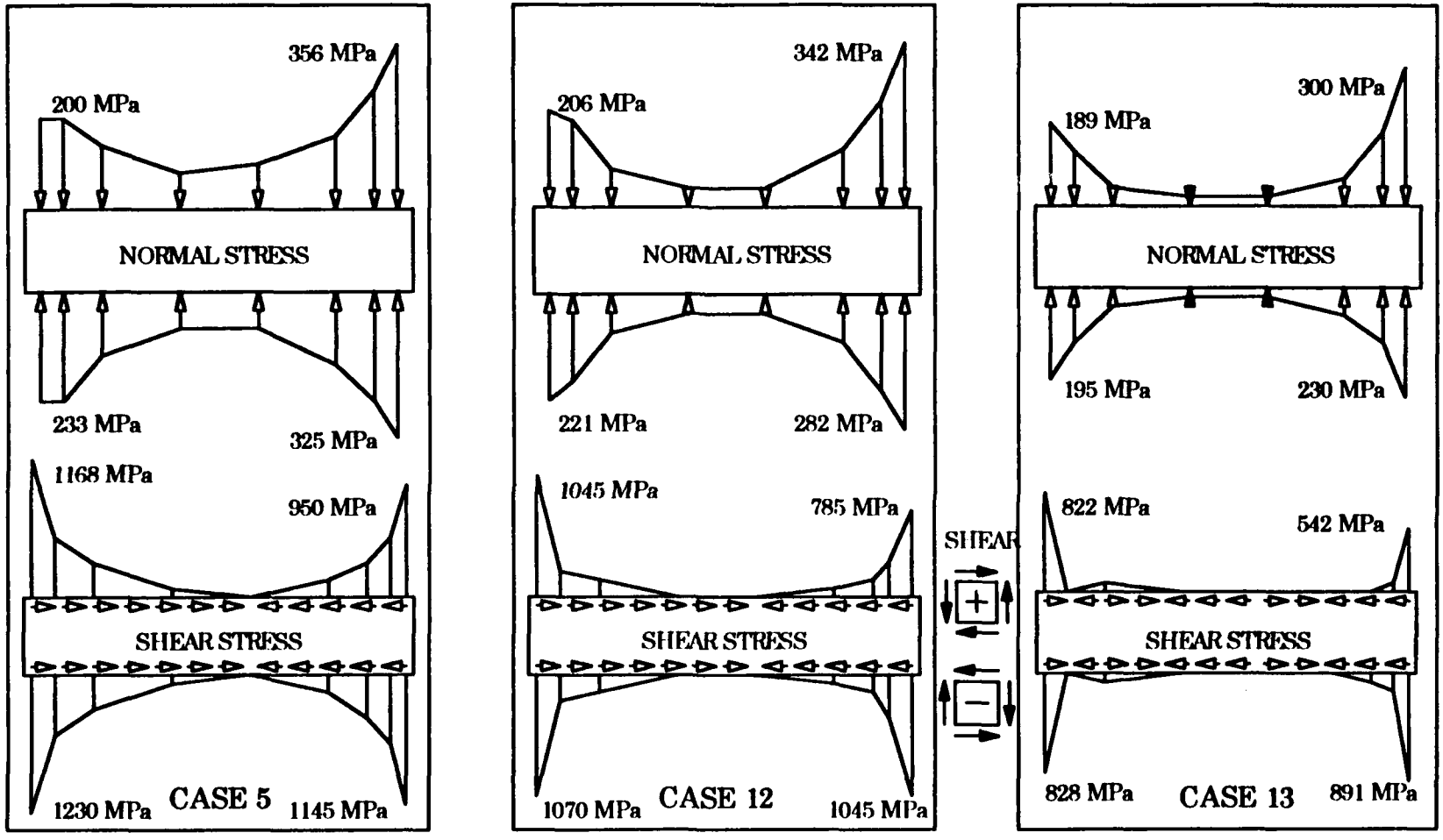

	Case5	Case 12	Case 13	Case 14	Case 15
Material B Height (mm)	1	0.5	0.25	0.1	0.05

$\alpha_A = 100 \times 10^{-6}/°C$ $\alpha_B = 300 \times 10^{-6}/°C$ $\alpha_C = 10 \times 10^{-6}/°C$ $E_A = E_B = E_C = 100$ GPa

Figure 4.6 Shear And Normal Stresses On The Midlayer For Cases 5, 12, 13, 14, And 15

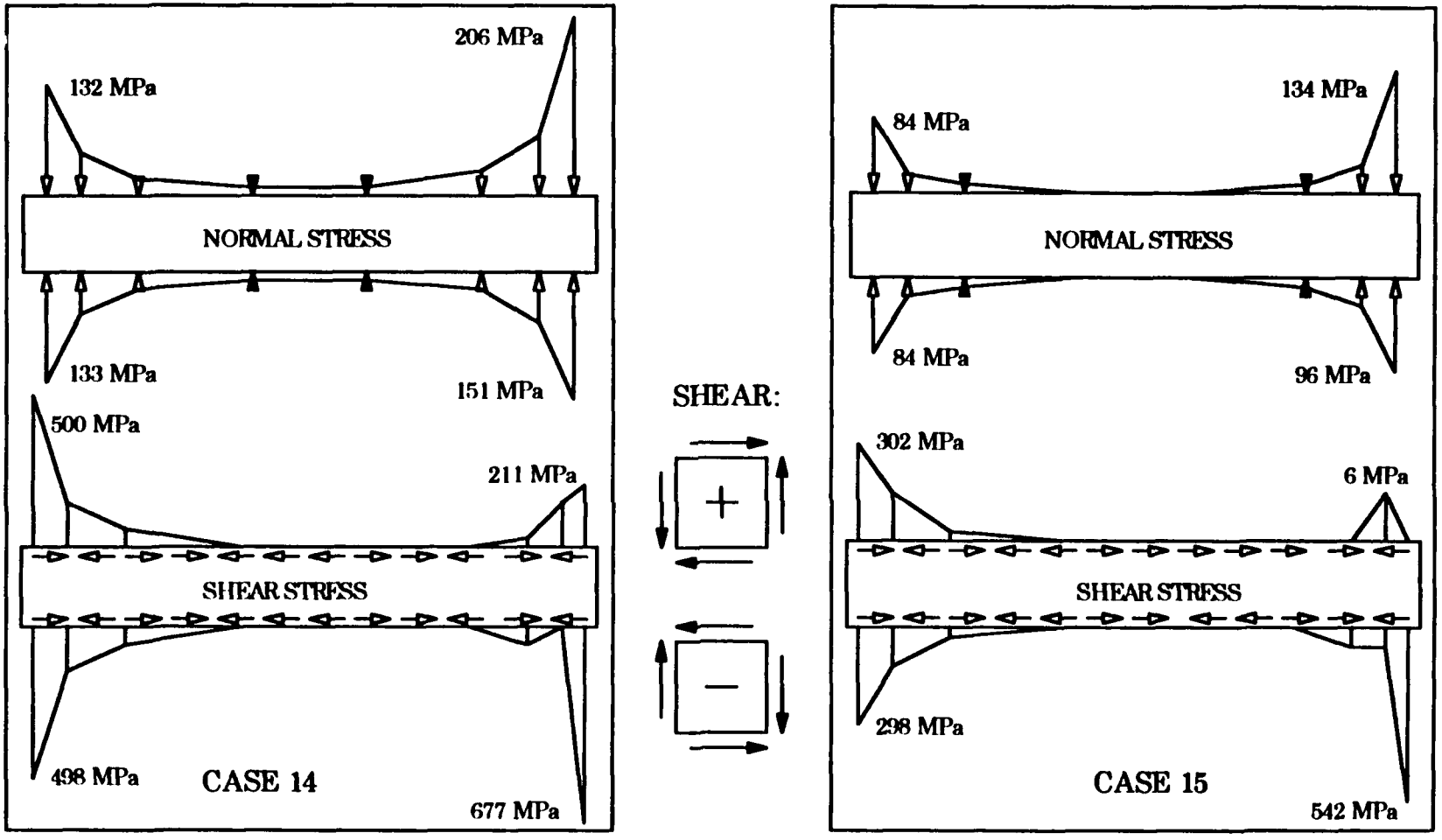

	Case 5	Case 12	Case 13	Case 14	Case 15
Material B Height (mm)	1	0.5	0.25	0.1	0.05

$\alpha_A = 100 \times 10^{-6}/°C$ $\alpha_B = 300 \times 10^{-6}/°C$ $\alpha_C = 10 \times 10^{-6}/°C$ $E_A = E_B = E_C = 100$ GPa

Figure 4.7 Shear And Normal Stresses On The Midlayer For Cases 14 And 15

CHAPTER 5. THE EFFECT OF MIDLAYER LENGTH ON SYSTEM BEHAVIOR

Here the effect of midlayer length on system behavior was investigated. The fixed values of layer thermal coefficients of expansion and thickness dimensions correspond to case 5. That is, the coefficients of thermal expansion of the top, mid and bottom layers are $100 \times 10^{-6}/^{\circ}C$, $300 \times 10^{-6}/^{\circ}C$, and $10 \times 10^{-6}/^{\circ}C$ respectively, and the thicknesses of each layer is fixed at 1 mm each. The results of six cases, (16, 17, 5, 18, 19, and 20) are compared. The sequence of these cases in decreasing magnitude of midlayer length is shown in Table 5.1 below. Figure 5.1 shows the geometry of these five cases to scale.

CASE	MIDLAYER LENGTH mm	FRACTION OF TOTAL
16	9.0	.90
17	7.5	.75
5	5.0	.50
18	2.5	.25
19	1.0	.10
20	.5	.05

Table 5.1 Geometry for the midlayer length study

The results of this study, shown in figures 5.2 through 5.4, are as follows.

- As in all previous studies, the shear stresses are significantly larger than the normal stresses.

- In all cases studied here, the normal stresses are bearing stresses.

- As the midlayer length decreases, the maximum interface normal and shear stresses increase until the midlayer length becomes 1 mm. A further decrease of the midlayer length decreases the stresses slightly.

- In all cases the maximum shear stress on the upper interface surface occurs at the inner corner point. The maximum shear stress on the lower interface also occurs at the inner corner point except for the least midlayer length case (case 20) where the maximum shear stress occurs at the outer corner point.

- The maximum shear stress occurs at the inner corner point of the lower interface surface for the three longest midlayer length cases (cases 17, 5, and 18). For the least midlayer length cases

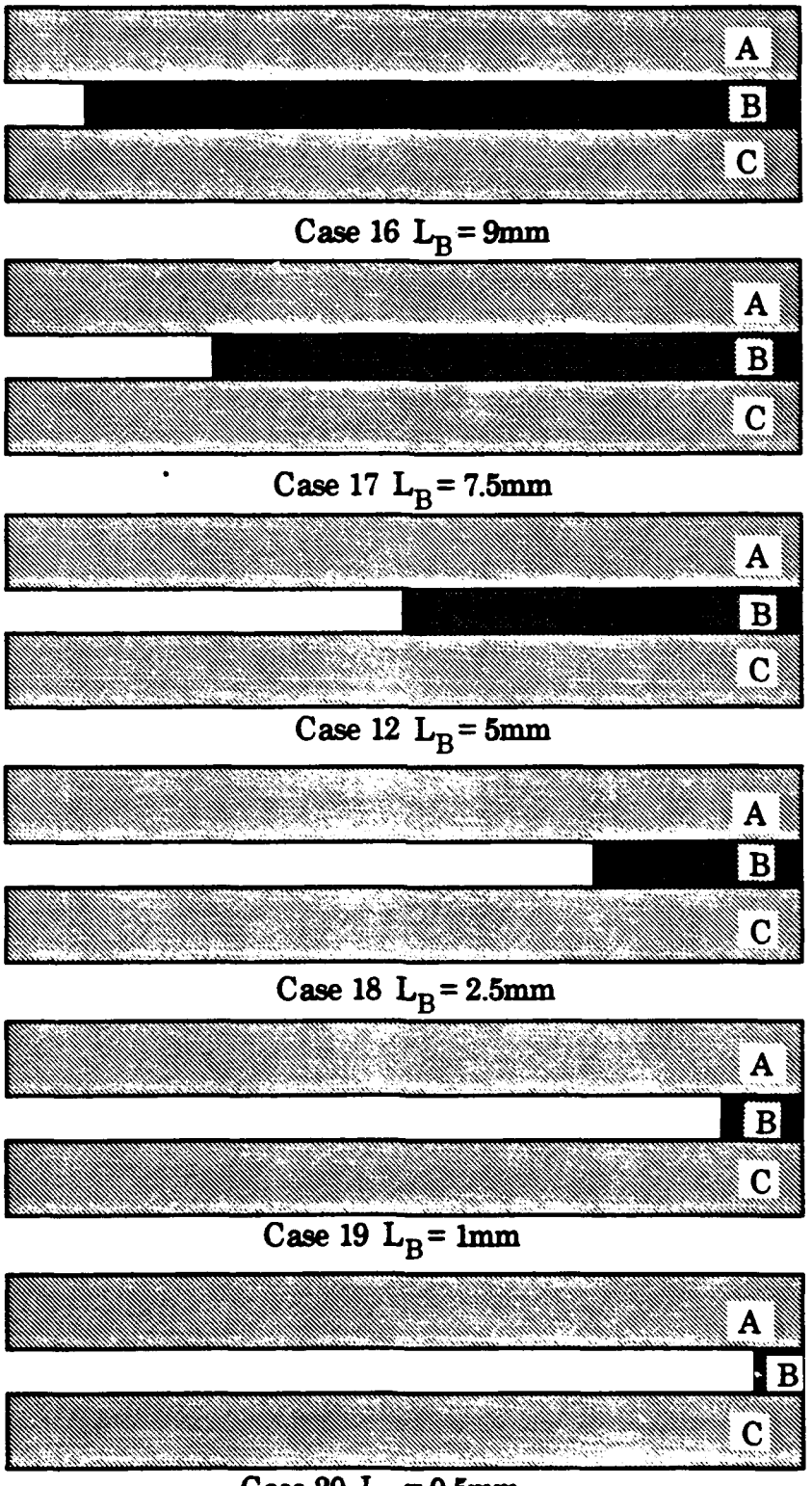

Figure 5.1 Tri-material Configurations For Cases 12, 16, 17, 18, 19, And 20

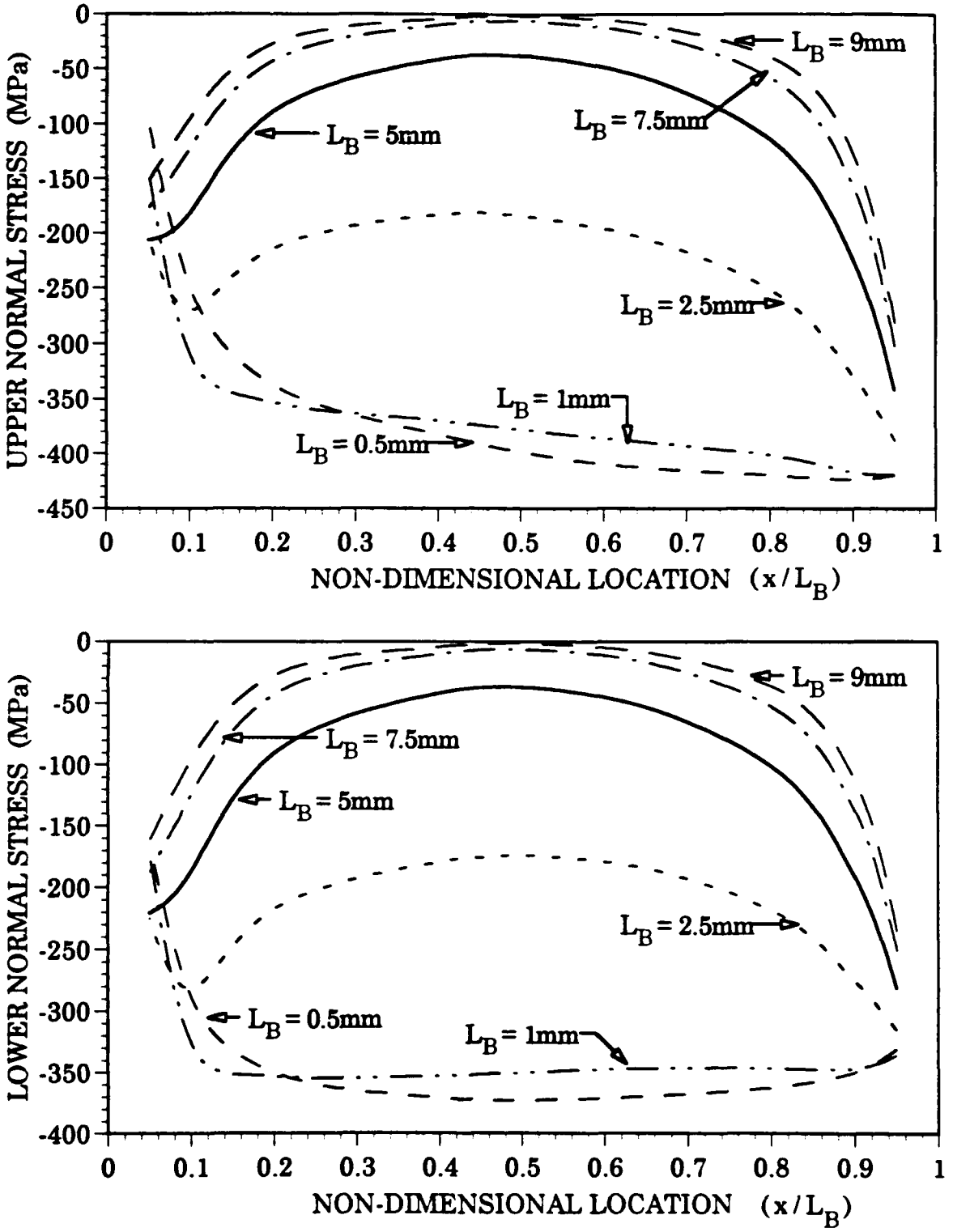

Figure 5.2 Normal Stress At Interfaces As A Function Of Non-dimensional Location For Cases 12, 16, 17, 18, 19, And 20

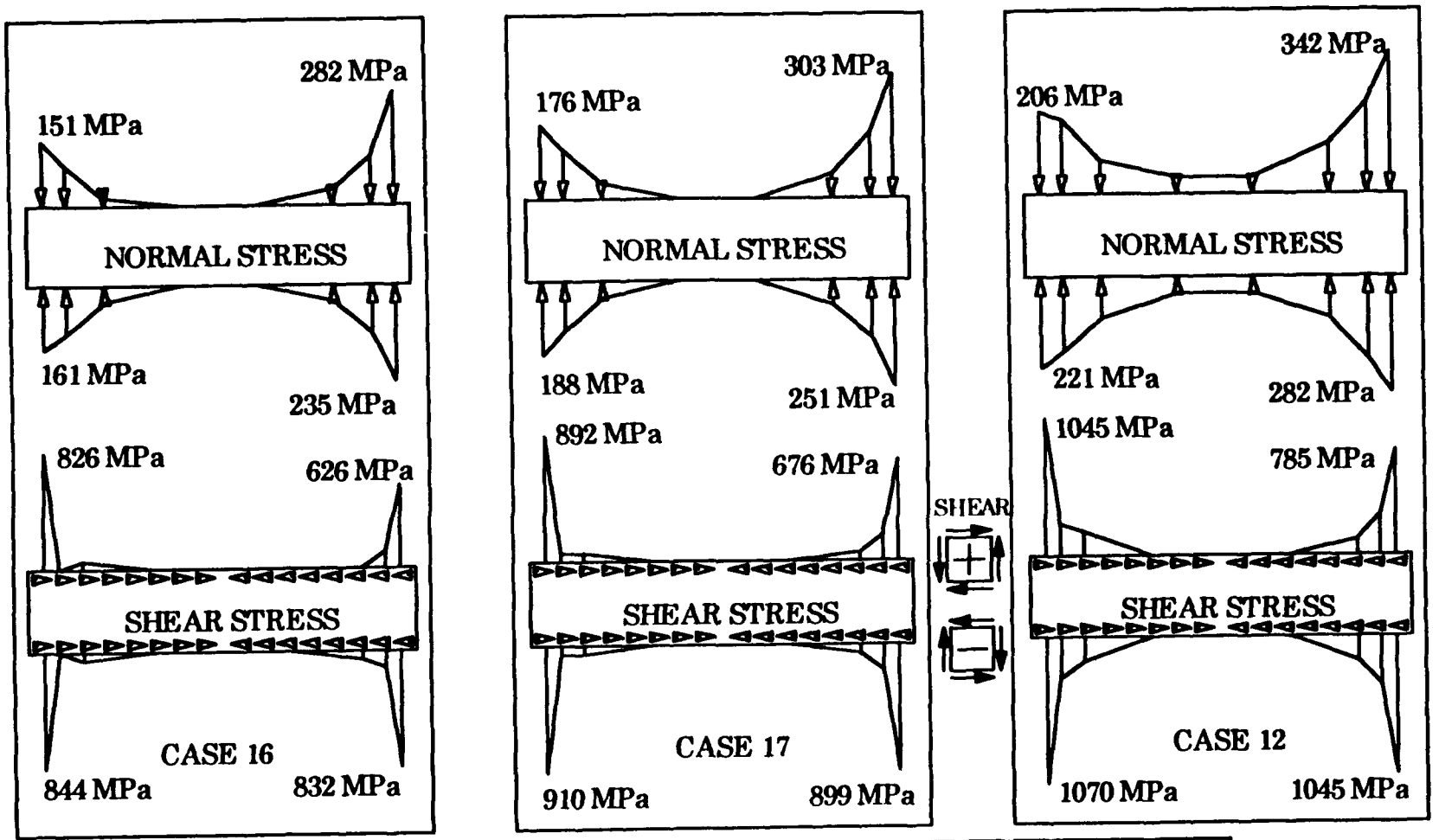

	Case 12	Case 16	Case 17	Case 18	Case 19	Case 20
Material B Length (mm)	5	9	7.5	2.5	1	0.5

$\alpha_A = 100 \times 10^{-6}/°C$ $\alpha_B = 300 \times 10^{-6}/°C$ $\alpha_C = 10 \times 10^{-6}/°C$ $E_A = E_B = E_C = 100$ GPa

Figure 5.3 Shear And Normal Stresses On The Midlayer For Cases 12, 16, And 17

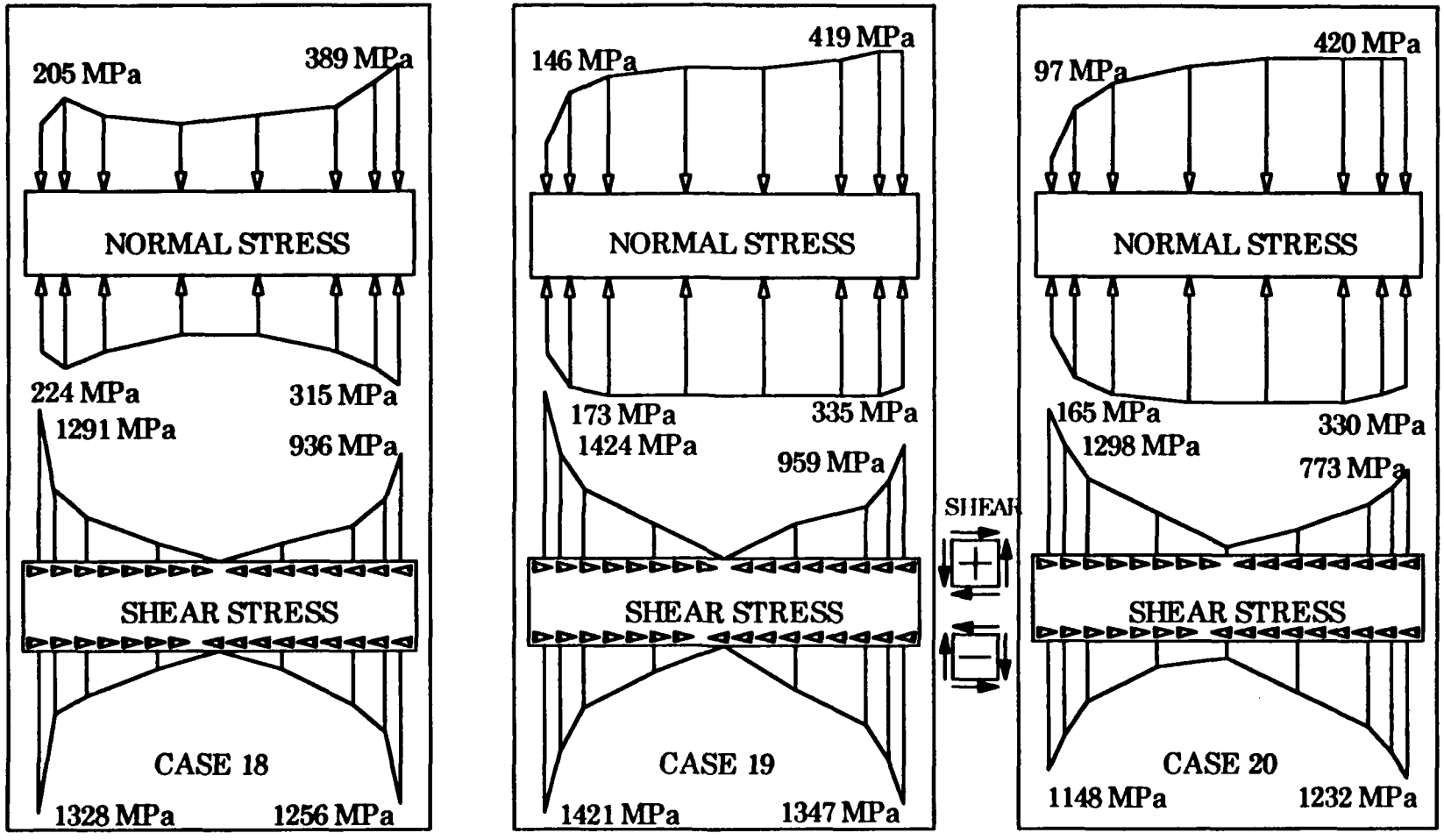

	Case 12	Case 16	Case 17	Case 18	Case 19	Case 20
Material B Length (mm)	5	9	7.5	2.5	1	0.5

$\alpha_A = 100 \times 10^{-6}/°C$ $\alpha_B = 300 \times 10^{-6}/°C$ $\alpha_C = 10 \times 10^{-6}/°C$ $E_A = E_B = E_C = 100$ GPa

Figure 5.4 Shear And Normal Stresses On The Midlayer For Cases 18, 19, And 20

(cases 19 and 20), the maximum shear stress occurs at the inner corner point of the upper interface surface.

- The maximum normal stresses occurs at the outer corner points of the upper and lower interface surfaces. The maximum normal normal stress on the upper interface surface is 10 to 30 percent larger than the maximum normal stress on the bottom surface.

Again it should be pointed out that the observations made above are for a particular trimaterial system. The locations and relative magnitudes of interface normal and shear stresses certainly depend on the selection of the thermal coefficients of expansion of each of the layers of the trimaterial system.

CHAPTER 6 THE EFFECT OF NONUNIFORM TEMPERATURE FIELD

This study investigated the effects of a nonuniform temperature field on a trimaterial electronic package where the top layer is a silicon chip, the bottom layer is a substrate and a thin solder midlayer is used to connect the chip to the substrate. In a thesis, Sapsai (4) undertook an exhaustive study of the thermal behavior of such electronic packages. A small part of the results obtained in that study is summarized here.

The geometry and thermal properties of the electronic package are prsented in Table 6.1 below.

	Length (mm)	Depth (mm)	CTE (/°C)	E (GPa)
CHIP	5.	2.	2.6×10^{-6}	133.
SOLDER	.5625	.2	29.0×10^{-6}	7.4
SUBSTRATE	5.6	2.	variable	variable

Table 6.1 Geometry and Material Properties of Three Layers

In table 6.1 CTE is the coefficient of thermal expansion, and E is Youngs modulus of elasticity. The Poisson's ratio's for the Silicon chip and the Pb-Sn solder are both 0.3.

The particular materials comprising the electronic package is a silicon chip in the top layer with a thermal conductivity coefficient equal to 150 W/mC , a Pb-Sn solder in the midlayer with a conductivity equal to 63 W/m . The bottom substrate layer varies among four materials, Alumina, Polymide fiberglass, Epoxy fiberglass, and Aluminum nitride (AlN). The properties of these four materials are presented in Table 6.2 below. The Poisson's ratio for all three substrates is 0.3.

SUBSTRATE	E (GPa)	CONDUCTIVITY	CTE (/°C)
ALUMINA	262	18. W/m°C	6.0×10^{-6}
POLYMIDE	40	.35 W/m°C	$14. \times 10^{-6}$
EPOXY	35	.16 W/m°C	$16. \times 10^{-6}$
AlN	339	230.	3.3×10^{-6}

Table 6.2 Material Properties of Three Substrates

The steady state thermal code discussed in Chapter 2 was used for the trimaterial electronic package with the geometry and material properties given in tables 6.1 and 6.2. The results obtained showed that the steady state temperature results was independent of the level of heat generation in the chip. It was also observed that the

substrate material governs the temperature profile through the package. The ratio of thermal conductivities has a significant effect on system behavior. A characteristic of low thermal conductivity substrates (i.e., $k_3/k_1 < .0025$, where subscript 1 denotes the top chip layer, and subscript 3 denotes the bottom substrate layer is that thermal gradients occur in both the lengthwise (x) and depthwise (y) directions. For high thermal conductivity substrates (i.e., $.1 < k_1/k_3 < 1.6$), the temperature field is uniform, that is, thermal gradients do not result. The reasons for these results are not presented here. The interested reader can refer to [4].

Figure 6.1 is a plot of thermal strain ϵ_t versus the nondimensional variable ϕ_y through the thickness of the trimaterial through the centerline of the three layers. The figure shows that there is no thermal strain gradients through either the chip or solder. It also shows the The thermal strain in the solder is much larger than the thermal strain in the chip regardless of the substrate material, as well as much larger than the thermal strain in the substrate in the case of the Aliminum nitrate and the Alumina substrates. In the case of the Epoxy fiberglass and Polymide fiberglass substrates, the thermal strain increases monotonically from the bottom of the substrate to the interface with the solder.

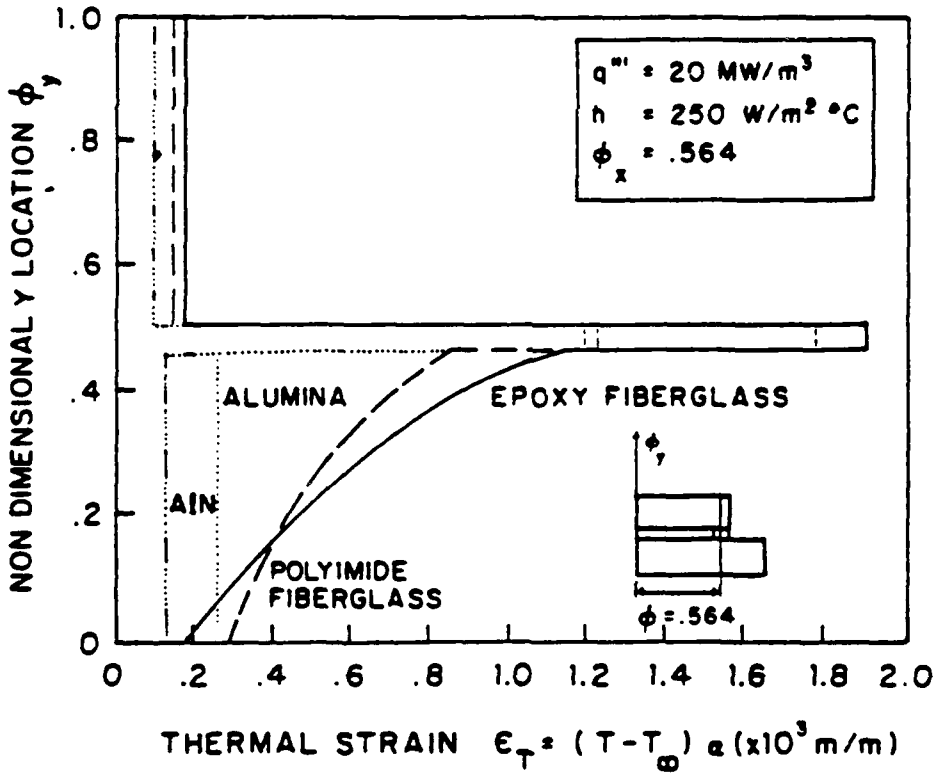

Figure 6.1 Thermal strain through the thickness of the trimaterial

The normal stress along the upper surface of the solder midlayer is shown in figure 6.2. The figure shows that the normal stresses are bearing in nature for all substrates. It is also seen that the bearing normal stresses on the upper solder surface are much larger, by a factor of 4, when Alumina or Aluminum nitrate substrates are used. In all cases, the maximum normal stress occurs close to the outer edge of the solder layer.

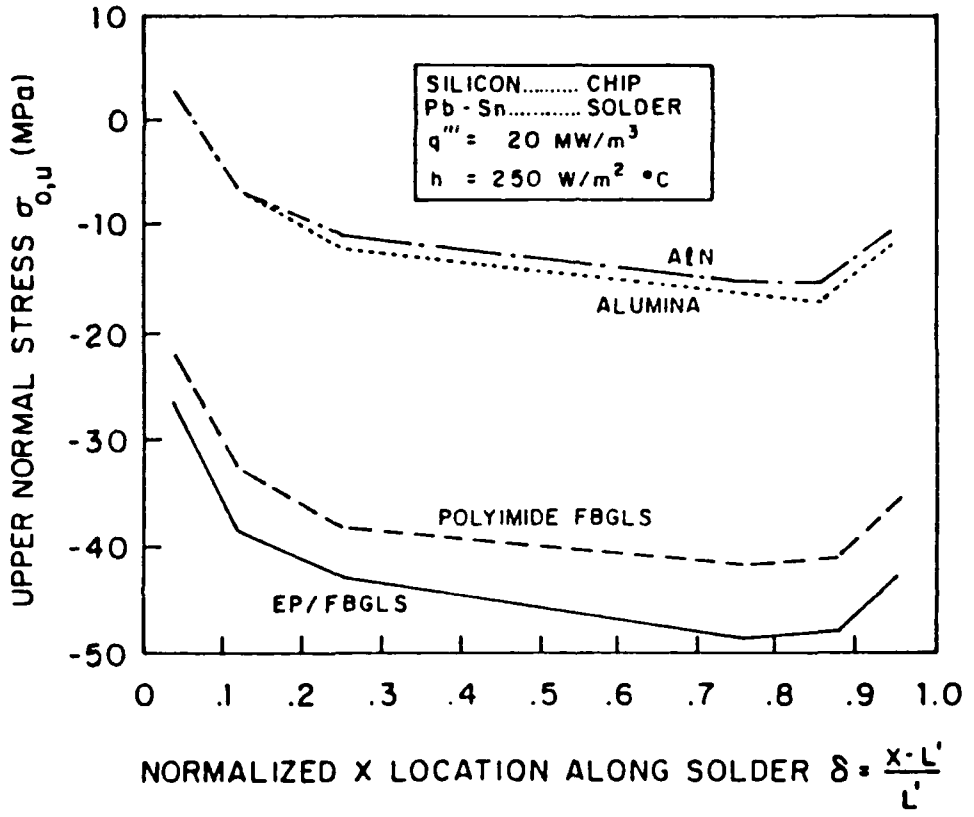

Figure 6.2 Normal Stress Along the Upper Solder Surface

Figures 6.3 and 6.4 show the shear stresses along the upper and lower surfaces of the solder midlayer. These figures show that on the upper surface, Alumina and Aluminum nitride substrates achieve their largest magnitude at the inside edge, while the shear stresses for the Epoxy fiberglass and Polymide fiberglass achieve their maximum at the outer edge. Reversal of this behavior occurs along the lower surface. Shear stress reversal (in direction) occurs at various locations. In all cases the shear stress distribution has a constant slope along the center two thirds span of the interface. The slopes of the shear stress distribution increase rapidly as the ends of the interface are approached. values at the inner and outer edges

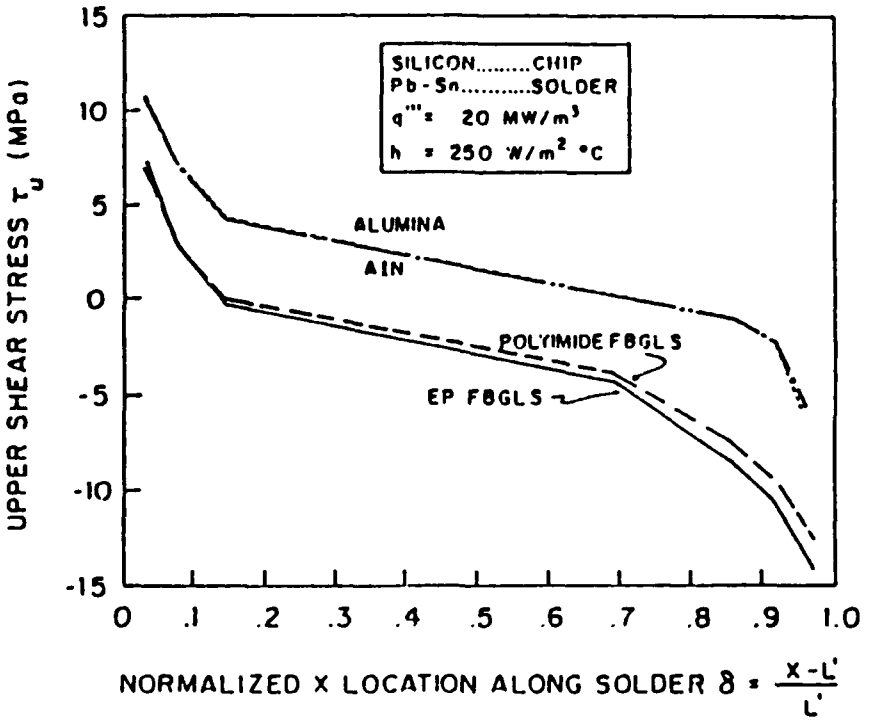

Figure 6.3 Shear Stresses Along the Upper Midlayer Surface

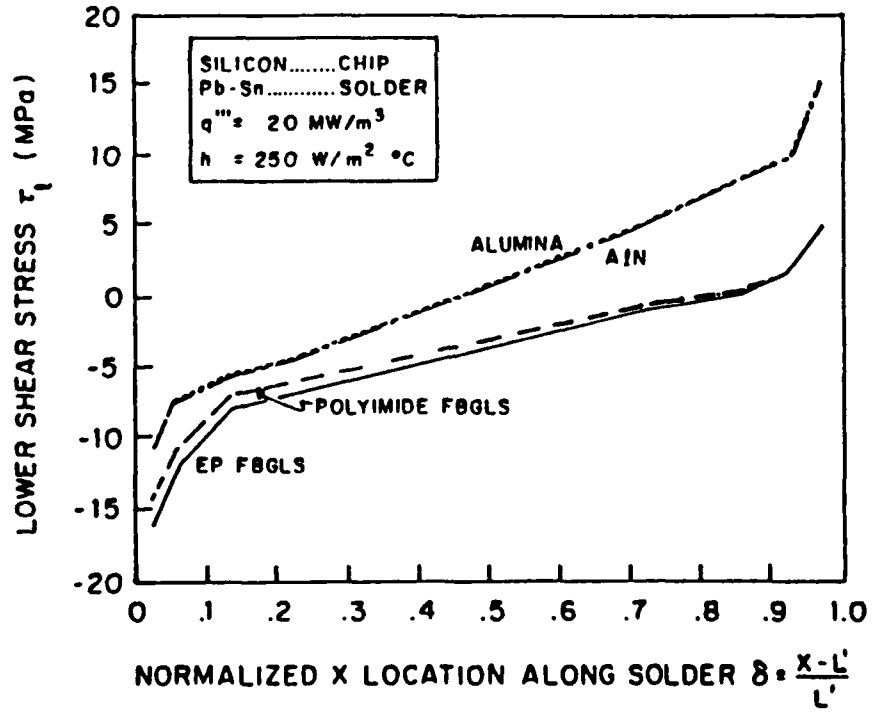

Figure 6.4 Shear Stresses Along the Lower Midlayer Surface

References

1. Timoshenko, S., Analysis of Bi-metal Thermostats, Journal of the Optical Society of America, Vol. 11, pp. 233-255, (1925).

2. Goland, M., and Reissner,E., The Stresses in Cemented Joints, Journal of Applied Mechanics, Transactions, ASME, 11, pp. 17-27, March, (1984).

3. Suhir, E., Advances in Thermal Modeling of Electronic Components and Systems, Volume 1, Chapter 5, pp. 337-412. Hemisphere Publishing Co., (1989).

4. Sapsai, A., Temperature Distribution and Thermally Induced Stresses in Electronic Packages, NPS, Dept. of Mechanical Engineering, Thesis for MS degree, September, 1992.

Distribution List

	Copies
Office of Naval Research Director, Technology (Code 02) 800 North Quincy Street Arlington, VA 22217-5000	1
Office of the Director of Defense Research and Engineering Information Office Library Branch The Pentagon, Rm. 3E 1006	1
Defense Technical Information Center Cameron Station Alexandria, VA 22314	2
Naval Postgraduate School Technical Library (Code52) Monterey, CA 93943-5100	2
Research Administration (Code 81) Naval Postgraduate School Monterey, CA 93943-5100	1
Professor M.D. Kelleher Dept. Of Mech. Engng. Naval Postgraduate School Monterey, CA 93943-5100	1
Prof. Y. W. Kwon Dept. of Mech. Engng. Naval Postgraduate School Monterey, CA 93943-5100	4
Prof. D. Salinas Dept. of Mech. Engng. Naval Postgraduate School Monterey, CA 93943-5100	4
Commanding Officer Naval Weapons Support Center (Code 0211) Crane, IN 47522	3